Cancer Letters 453 (2019) 57–73

Contents lists available at ScienceDirect

Cancer Letters

journal homepage: www.elsevier.com/locate/canlet

Original Articles

Cardiac glycoside cerberin exerts anticancer activity through PI3K/AKT/mTOR signal transduction inhibition

Md Shahadat Hossan[a,b,*], Zi-Yang Chan[b], Hilary M. Collins[a], Fiona N. Shipton[b], Mark S. Butler[c], Mohammed Rahmatullah[d], Jong Bong Lee[e], Pavel Gershkovich[a], Leonid Kagan[e], Teng-Jin Khoo[b], Christophe Wiart[b], Tracey D. Bradshaw[a,**]

[a] School of Pharmacy, Centre for Biomolecular Sciences, The University of Nottingham, University Park, Nottingham, NG7 2RD, UK
[b] School of Pharmacy, University of Nottingham Malaysia Campus, Jalan Broga, Semenyih, 43500, Selangor, Malaysia
[c] Institute for Molecular Bioscience, University of Queensland, St. Lucia, QLD, 4072, Brisbane, Queensland, Australia
[d] Department of Pharmacy, University of Development Alternative, Lalmatia, Dhaka, 1207, Bangladesh
[e] Department of Pharmaceutics, Ernest Mario School of Pharmacy, Rutgers, The State University of New Jersey, Piscataway, NJ, 08854, USA

ARTICLE INFO

Keywords:
Cardenolide
DNA damage
Apoptosis
Reactive oxygen species
Cerbera odollam

ABSTRACT

Natural products possess a significant role in anticancer therapy and many currently-used anticancer drugs are of natural origin. Cerberin (CR), a cardenolide isolated from the fruit kernel of *Cerbera odollam*, was found to potently inhibit cancer cell growth (GI_{50} values < 90 nM), colony formation and migration. Significant G2/M cell cycle arrest preceded time- and dose-dependent apoptosis-induction in human cancer cell lines corroborated by dose-and time-dependent PARP cleavage and caspase 3/7 activation, in addition to reduced Bcl-2 and Mcl-1 expression. CR potently inhibited PI3K/AKT/mTOR signalling depleting polo-like kinase 1 (PLK-1), c-Myc and STAT-3 expression. Additionally, CR significantly increased the generation of reactive oxygen species (ROS) producing DNA double strand breaks. Preliminary *in silico* biopharmaceutical assessment of CR predicted > 60% bioavailability and rapid absorption; doses of 1–10 mg/kg CR were predicted to maintain efficacious unbound plasma concentrations (> GI_{50} value).

CR's potent and selective anti-tumour activity, and its targeting of key signalling mechanisms pertinent to tumourigenesis support further preclinical evaluation of this cardiac glycoside.

1. Introduction

Cancer causes mortality and morbidity worldwide, with an estimated 18.1 million new cases and 9.6 million deaths in 2018 [1]. Carcinomas, cancers of epithelial origin comprise > 200 diseases alone. Cancer pathogenesis is complex; molecularly-targeted and cytotoxic chemotherapy agents are combined in the treatment regimens of multiple systemic and metastatic malignancies [2,3]. However, adverse side effects and drug resistance are obstacles to curative treatment and motivate research to discover new and safe therapies. Natural products (NPs) play a crucial role in drug discovery, with > 50% of clinically approved drugs sourced from, or inspired by nature [4]. Efficacious anticancer drugs including taxanes, vincristine and etoposide are plant-derived. The purpose of research described herein is to elucidate mechanisms that underlie the potent, yet selective activity of cerberin (CR), a plant-derived cardiac glycoside, and to identify its molecular targets.

CR was originally isolated and characterised from the seed kernels of a Southeast Asian tree, *Cerbera odollam* [5]. *C. odollam* is well-known within Southeast Asia to be poisonous, with restricted ethnobotanical uses as a purgative and rat poison [6]. Many instances of human fatalities have been attributed to the plant, with CR named as the principle toxin [7]. CR and *C. odollam* extracts have been shown to be potently cytotoxic against different cancer cell lines [8–12], but the exact mechanism(s) of action have not been examined. Cardiac glycosides are comprised of a 17 carbon steroidal backbone linked to a sugar moiety *via* a glycosidic bond, they differ through alterations in the steroidal and glycosidic moieties. CR has a five-membered lactone ring and a distinctive sugar moiety identified as 2′−*O*-acetyl-L-thevetose [5,8,11]. Cardiac glycosides like digoxin and ouabain are known for their inhibitory actions on the Na^+/K^+-ATPase transmembrane ion pump, leading to a positive inotropic effect on the heart. Digoxin

* Corresponding author. Centre for Biomolecular Sciences, The University of Nottingham, University Park, Nottingham, NG7 2RD, UK.
** Corresponding author. Centre for Biomolecular Sciences, The University of Nottingham, University Park, Nottingham, NG7 2RD, UK.
E-mail addresses: bdshahadat@yahoo.com (M.S. Hossan), tracey.bradshaw@nottingham.ac.uk (T.D. Bradshaw).

https://doi.org/10.1016/j.canlet.2019.03.034
Received 8 November 2018; Received in revised form 14 March 2019; Accepted 20 March 2019
0304-3835/ © 2019 Elsevier B.V. All rights reserved.

(Lanoxin®) is widely indicated for the treatment of congestive heart failure despite having a narrow therapeutic window [13]. During the last two decades, the antiproliferative and apoptotic effects of various cardiac glycosides have become apparent. Many plant derived cardiac glycosides like convallatoxin, digoxin, peruvoside, oleandrin, ouabain and strophantidin have been shown to exert *in vitro* anticancer effects [10,14,15]. Due to their anticancer activity at low nanomolar concentrations against many cancer cell types, cardiac glycosides have been proposed as potential anticancer agents [16,17]. However, CR's potential as an anticancer agent has yet to be explored and no data reporting anticancer mechanisms have been reported. In this study, the effects of CR were investigated against a panel of cancer cell lines; further studies focussed upon pancreatic (PANC-1), triple negative breast (MDA-MB-468) and non-small cell lung (A549) carcinoma cell lines for extensive biological evaluation and elucidation of the mechanism(s) of action.

2. Materials and methods

2.1. Plant collection and extraction

The matured fruits of *Cerbera odollam* (20 kg) were collected in the autumn of 2015 from Penang, Malaysia. All plant specimens were positively identified as *C. odollam* and a voucher specimen (SH_UNMC-069B) was deposited in the herbarium of the School of Pharmacy, University of Nottingham Malaysia Campus. The fruits of *C. odollam* were cut open to retrieve the seeds from which their kernels were exposed and dried in an oven with aeration at 45 °C for 1 week. The dried seed kernels (500 g) were ground and extracted with 9:1 dichloromethane: methanol to yield a dark brown crude extract (15 g).

2.2. Isolation of cerberin

The crude kernel extract of *C. odollam* was dissolved in methanol (200 mL) and partitioned against petroleum ether (3 × 100 mL) to remove fatty constituents. The methanol-soluble fraction was recovered and dried *in vacuo* to yield a brown amorphous solid extract (9.5 g), which was separated using preparative layer chromatography (PLC, Silica Gel 60 Merck 7759, 230-400 mesh) with ethyl acetate-hexane-methanol (9:1:0.2) as the eluent and visualised under UV light at 254 nm. A distinctively separated band (R_f 0.25) on the PLC plate was scraped off and extracted with 200 mL dichloromethane-methanol (9:1) to yield a white amorphous solid (30 mg). The isolated compound was analysed with a Waters ACQUITY®ARC UHPLC system equipped with Waters Quaternary Solvent Manager-R, Sample Manager FTN-R and 2998 PDA Detector. The separation was conducted on a Waters CORTECS® C18 column (4.6 × 50 mm, 2.7 µm) with a mobile phase of A (H_2O, 0.1% TFA) and B (ACN) under gradient elution of 10–90% B over 30 min at a flow rate of 1 mL/min. Total injection volume was 5 µL (5 mg/mL CR stock solution in ACN). Two different chromatograms with PDA detection at 254 nm and MaxPlot (200-400 nm) were generated. ^{1}H NMR spectrum of the pure sample was obtained in CD_3OD on a Bruker 600 MHz NMR spectrometer, using TMS as internal standard.

2.3. Cell culture

CR activity was tested against a panel of cancer cells derived from breast (MCF-7, MDA-MB-231, MDA-MB-468 and SKBR3), colon (HT-29, HCT-116 and vincristine-resistant- (VR)—HCT-116), pancreatic (PANC-1 and MIA PaCa-2), lung (A549), liver (HepG2) and nasopharyngeal (HK1) carcinomas. All cell lines were obtained from the American Type Culture Collection (ATCC) except for the HK1 and NP-69 cell lines which were a gift from Prof. GSW Tsao, Faculty of Medicine, The University of Hong Kong [18]. The VR-HCT-116 cell line was developed at the University of Nottingham following continued exposure (> 6 months) of the HCT-116 cell line to escalating concentrations of vincristine [19]. Cell cultures were maintained in RPMI 1640 (Gibco) supplemented with sodium bicarbonate (2 g/L), 10% foetal bovine serum (FBS) (Gibco) and 2 mL-glutamine (Gibco) under a humidified atmosphere containing 5% CO_2 in air at 37 °C. The VR-HCT-116 cell line was subcultured additionally in the presence of 2 µM vincristine. Cells were passaged twice weekly upon reaching 70–80% confluency.

2.4. MTT assay

The 3-(4,5-dimethylthiazol-2-yl)-2,5-diphenyltetrazolium bromide (MTT) assay was adapted from a previously-established protocol [20]. Briefly, cells were seeded at a density of 3×10^3 cells per well into 96-well plates (Nunc, Roskilde, Denmark) 24 h prior to treatment with test agents at serially-diluted concentrations. MTT assays were performed at the time of agent addition (T zero) following 72 h exposure of cells to test agents [21]. GraphPad Prism 7.04 (Graphpad Software Inc, USA) and Microsoft Office 365 were used for generating curves and obtaining 50% Growth inhibition (GI_{50}) values. Results are expressed as the mean of total ≥4 independent experiments (n = 6).

To authenticate MTT assay results, cell counts were performed. Briefly, into 6-well plates 2×10^4 cells were seeded and incubated overnight before treatment with CR at 4-5 different concentrations proximate to GI_{50} values (obtained by MTT assay following 72 h exposure). The cells were incubated with the test agent for 72 h, harvested and counted using a haemocytometer [19].

2.5. Clonogenic assay

The clonogenic assay is an *in vitro* cell survival assay that measures the ability of single cells to survive and retain proliferative capacity to form progeny colonies after brief exposure to test compounds [22]. The assay was performed according to our previously described procedure [19,21].

2.6. Migration assay

Migration assays were performed to measure the ability of test agents to inhibit the migration of cancer cells. Cells were seeded in 6-well plates at a density of 1×10^6 in 2 mL medium supplemented with 10% FBS and allowed to grow until 90% confluent. A scratch or "wound" was formed using a sterile 200 µL pipette tip. Subsequently, cells were washed with phosphate-buffered saline (PBS) and incubated with the test compound at 2 × GI_{50} concentration in the presence of FBS (10%) for 48 h. Acquisition of microscopy images was carried out using an inverted microscope (Nikon ECLIPSE TS100) equipped with a Nikon COOLPIX 4500 camera at 0, 24 and 48 h. Images were analysed using ImageJ software (NIH, Maryland, USA). Results were expressed as a percentage of the original wound area [23].

2.7. Cell cycle analysis

Cell cycle analyses were carried out as described [23]. Briefly, cells were seeded in 6-well plates at densities of 0.5–1 × 10^6 cells/well. Following treatment, cells were harvested, centrifuged and then re-suspended in 0.3–0.5 mL fluorochrome solution containing 50 µg/mL propidium iodide (PI), 0.1 mg/mL Ribonuclease A, 0.1% v/v Triton X-100, and 0.1% w/v sodium citrate in deionised water (dH_2O). Cells were stored overnight in the dark at 4 °C. Cell cycle analyses were performed on a Beckman Coulter FC500 flow cytometer (Indianapolis, IN, USA). Weasel flow cytometry analysis software (v 3.5) (WEHI, Melbourne, VIC, Australia) was used to analyse the data.

2.8. Detection of DNA double strand breaks

γH2A.X foci appear at the sites of DNA double-strand breaks (DSBs) and therefore represent a biomarker of DNA DSB damage [24].

Detection of γH2A.X foci was carried out as reported previously [23,25]. Cells were seeded at a density of 1–1.5 × 10^6 in 10 cm^2 dishes and allowed to adhere for 24 h at 37 °C. Cells were treated with 1 × and 2 × GI_{50} of CR for 24 and 48 h. Cells were then harvested and fixed with 1% methanol-free formaldehyde in PBS. Cells were then incubated for 5 min at room temperature and permeabilised using 0.4% Triton-X-100 in PBS (500 μL). Cells were rinsed with PBS, centrifuged and re-suspended in 200 μL γH2A.X 1° Ab (EMD-Millipore, 1:3333 dilution) and incubated for 1.5 h at room temperature. Goat anti-mouse Alexa Fluor 488 2° Ab (1:1750 dilution) was later added and cells incubated at room temperature for 1 h in the dark. Cells were washed with PBS and then resuspended in 300 μL solution of 50 μg/mL PI/0.1 mg/mL RNase A in PBS followed by incubation for ≥10 min at room temperature. A Beckman Coulter Cytomics FC500 MCL flow cytometer (Indianapolis, IN, USA) was used to take the measurements; data were analysed *via* Weasel flow cytometry analysis software (v 3.5) (WEHI, Melbourne, VIC, Australia).

2.9. Annexin V-FITC and propidium iodide apoptosis assay

Cells were seeded in 12-well plates at densities of 1.5 × 10^5 cells/well (24 h), 1 × 10^5 cells/well (48 h) and 5 × 10^4 (72 h). Cells were incubated overnight prior to exposure to CR at 1 × and 2 × GI_{50} concentration for 24 h −72 h. Following treatment, cells were trypsinised, centrifuged, collected in FACS tubes and kept on ice for 10 min in 2 mL cold medium. Following centrifugation, cells were washed with ice-cold PBS, then pelleted by centrifugation. Annexin-V-FITC (5 μL) plus 100 μL 1 × annexin-V buffer was added to cells; after 15 min incubation in the dark at room temperature, PI (10 μL; 50 μg/mL in PBS) plus 400 μL annexin-V buffer was added. Cells were placed on ice and kept in the dark for 10 min prior to analyses using Beckman Coulter FC500 flow cytometer (Indianapolis, IN, USA). Weasel flow cytometry analysis software was used to evaluate data (v 3.5) (WEHI, Melbourne, VIC, Australia).

2.10. Caspase-3/7 activity assay

The caspase 3/7 assay kit (Promega) was used to determine caspase activity as previously reported [23]. Briefly, cells (5 × 10^3 per well) were seeded in white opaque 96-well plates and incubated overnight at 37 °C. CR or vincristine was introduced at 1 × GI_{50}. Caspase-Glo 3/7 reagent was added to the cells in a 1:1 ratio of reagent to cell culture medium. An orbital shaker was used to mix the reagent. Plates were incubated for 60 min at room temperature. The resulting luminescence was read using the Envision 2104 multi-label plate reader (PerkinElmer, Waltham, MA, USA).

2.11. Western blots

Western blotting was carried out as previously described [23]. Cells were seeded in 10 cm^2 dishes at a density of 1–2 × 10^6 per dish and allowed to attach for 24 h prior to exposure to 1 × GI_{50} and 2 × GI_{50} CR. Following the desired treatment period cell lysates were prepared and protein concentrations were calculated by Bradford assay [26]. Protein (50 μg per sample) was separated using the SDS PAGE and transferred to the nitrocellulose membrane. Whole PARP, cleaved PARP, Mcl-1, Bcl-2, PLK1, p-mTOR, mTOR, p-4EBP1, 4EBP1, *p*-Akt, Akt, p-p53, p53, *p*-eIF4e, eIF4e, c-MYC, MAPK ERK1/2, *p*-ERK1/2, p-STAT3, STAT-3 and GAPDH 1° antibodies (Abs) were purchased from Cell Signalling Technology (Danvers, MA, USA). Anti-rabbit and anti-mouse immunoglobulin G (IgG) horseradish peroxidase-conjugated 2° Abs were obtained from Dako (Santa Clara, CA, USA). Proteins were detected by immunoblotting, as previously described [27]. ImageJ software (NIH, Maryland, USA) was used for densitometric analyses.

2.12. Confocal microscopy

Confocal imaging was conducted as described [28]. All procedures were performed at room temperature unless stated otherwise. Cells at a density of 1 × 10^4 were seeded in 8-well μ-slides (Ibidi, Planegg, Germany) in 200 μL medium and incubated overnight to adhere. Following 24 h treatment, cells were fixed with formaldehyde (3.7% in PBS; 10–15 min). Cells were then permeabilised by PBT (PBS + 0.1% Triton X-100; 2–3 min). To prevent non-specific protein binding cells were blocked for 1 h using PBT and 1% bovine serum albumin (BSA). Cells were incubated for 2 h with 1° monoclonal anti-α-tubulin Ab (Thermo Scientific), washed with PBT and incubated in the dark for 1 h with fluorescent 2° Ab (anti-mouse IgG Alexa Fluor® 488 F, 1:500 dilution). DNA binding dye DRAQ5 (1:3000) was added and cells were incubated for 5 min in the dark. Cells were visualised and images captured using a Zeiss LSM510 Meta confocal microscope conjugated with Zeiss LSM image browser software (version 4.2.0.121).

2.13. Detection of reactive oxygen species

To measure the H_2O_2 levels in cells, the rapid ROS-Glo™ H_2O_2 luminometric-based assay (Promega, UK) was adapted. Briefly, 5 × 10^3 cells were seeded in white opaque 96-well plates in 80 μL medium, incubated overnight and then treated with CR or vincristine for 24 h H_2O_2 substrate (25 μM) was added to the cells 30 min before completion of the 6 h incubation period; 100 μL ROS-Glo™ detection solution was then added, and samples were incubated for 20 min at room temperature. Relative luminescence was measured using an Envision 2104 multilabel plate reader (PerkinElmer, Waltham, MA, USA).

2.14. In silico pharmacokinetic analyses

In silico prediction of CR pharmacokinetics was performed using GastroPlus™ v9.5.0004 (SimulationsPlus, Lancaster, CA, USA) with built-in ADMET Predictor™ v8.1.0.0. All physicochemical and biopharmaceutical properties were predicted from the chemical structure, specific input parameters for the simulations can be found in the supplementary information (Supplementary Table S1). Advanced compartmental and transit (ACAT) and physiologically-based pharmacokinetic (PBPK) models were used with physiological parameters of a 0.025 kg mouse for the simulations. Paracellular permeability and enterohepatic circulation were turned on, and log D was estimated by structure-based model v6.1. Hepatic clearance (CL_h) was simulated with recombinant CYP predictions from the ADMET Predictor™. Renal clearance (CL_r) was predicted by the product of fraction unbound in plasma and glomerular filtration rate. Simulations were performed for i.v., p.o. and s.c. administration routes.

2.15. Statistical analyses

Experiments were conducted ≥3 times and representative experiments are shown in the Figures. One-way and two-way analyses of variance (ANOVAs) were used to determine statistical significance. Levels of significance (*, $p < 0.05$; **, $p < 0.01$; ***, $p < 0.001$; and ****, $p < 0.0001$ compared to untreated control) were determined using Dunnett's multiple comparison test.

3. Results

3.1. Characterisation of cerberin from Cerbera odollam

Isolated CR (section 2.2) was positively characterised by comparison of its ^{1}H NMR spectral data with available literature [8,9,29–31] (Supplementary Fig. 1; Supplementary Table S2). The ^{1}H NMR spectrum of CR showed a distinctive methyl singlet resonance at δ_H

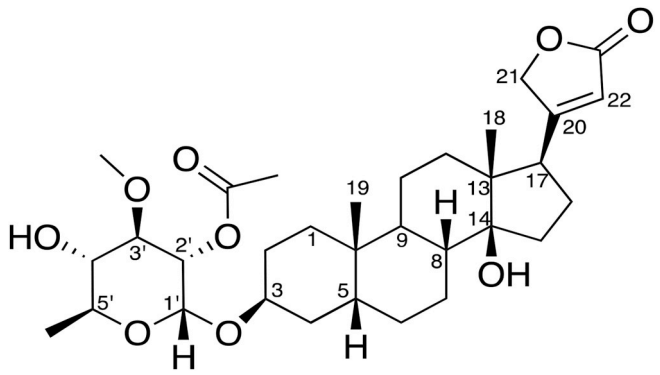

Fig. 1. Structure of cerberin (CR).

2.05 ppm, corresponding to its 2′—*O*-acetyl substituent (H-2′) (Fig. 1). A methoxy methyl singlet resonance (H-3′) detected at δ_H 3.57 ppm indicated the glycosidic moiety of CR to be 2′—*O*-acetyl-L-thevetose as reported in the literature [9,29,32]. An α,β-unsaturated-γ-lactone moiety of the cardenolide skeleton in CR was readily determined based on an olefinic proton resonance detected at δ_H 5.89 ppm (H-22), which was coupled to two downfield methylene proton resonances at δ_H 4.82 (H-21′) and δ_H 4.98 ppm (H21″) respectively. The stereochemistry of H-17 was established as 17β due to its chemical shift at δ_H 2.83 ppm, consistent with published data on 17β cardenolide isomers such as 17β neriifolin [11,30] (Supplementary Table S2). The CR sample was tested and found to be pure *via* UHPLC analysis, which showed a single well resolved peak at R_t13.04 min (PDA 254 nm, PDA MaxPlot 200–400 nm) (Supplementary Fig. S6).

3.2. Growth inhibitory effect of Cerbera odollam extract

The growth inhibitory activity of the defatted dichloromethane: methanol (9:1) extract of *C. odollam* fruits was initially tested against 9 cancer cell lines derived from 6 distinct organ sites using the MTT assay. Treatment with the extract revealed various growth inhibitory activities against all the cell lines tested (Table 1). Statistical analyses between control and treatment groups revealed significant ($p < 0.001$) growth inhibition following treatment with extract concentrations ≤0.01 μg/mL in all the cancer cell lines tested except MDA-MB-231 which showed significant growth inhibition at concentrations of ≤0.5 μg/mL. The extract exhibited 50% *in vitro* growth inhibitory (GI_{50}) activities between 0.03 and 0.17 μg/mL in all tested carcinoma cell lines. Growth inhibition by *C. oddolam* extract was examined in non-tumourigenic MRC-fibroblasts. The GI_{50} value of 146 μg/mL revealed large cancer-selectivity indices (SI; between 858- and 4866-fold). Subsequently, the pure compound CR was isolated from this extract; the anticancer activity of CR was then rigorously examined, and elucidation of anticancer mechanisms of action undertaken.

3.3. MTT assay results: evaluation of the cytotoxic potential of CR in a panel of cancerous vs non-transformed human cells

The *in vitro* antitumour activity and selectivity of CR was tested against a panel of cell lines derived from breast, colon, pancreatic, lung, liver and nasopharyngeal cancers, MRC-5 fibroblasts and NP-69 nasopharyngeal epithelial cells by MTT assay. CR elicited a concentration-dependent decrease in the number of viable cells (exemplified for PANC-1 and A549 in Fig. 2A) and exhibited potency against all the cancer cell lines tested. Similar to the *C. odollam* extract, significant growth inhibition (determined by a two-way ANOVA between control and treatment groups) was evoked by nanomolar concentrations of CR in all cancer cell lines tested. The vehicle control DMSO did not affect absorbance readings in any of the cell lines (data not shown). The GI_{50} values for CR against 12 cancer cell lines ranged between 22.23 nM

Table 1
Effect of *C. odollam* extract on the growth of human-derived cancer cells.

Cells	Breast carcinoma			Colon carcinoma		Pancreatic carcinoma	Nasopharyngeal carcinoma	Small lung carcinoma	Liver carcinoma	Human foetal lung fibroblast cells
	MCF-7	MDA-MB-231	SKBR-3	HCT-116	HT29	Panc-1	HK-1	A549	HepG2	MRC-5
Mean GI_{50} ± SD (μg/mL)[a]	0.062 ± 0.006	0.17 ± 0.02	0.088 ± 0.009	0.03 ± 0.005	0.07 ± 0.01	0.06 ± 0.017	0.03 ± 0.67	0.05 ± 1.00	0.05 ± 1.43	146 ± 1.56
SI[b] compared to the **MRC-5** cells	2354	858	1659	4866	2085	2212	4866	2920	2920	

Mean ± SD GI_{50} values were determined by MTT assays following 72 h exposure of cells to *C. odollam* extract (n = 4) and expressed as a mean ± SD of ≥ 3 independent trials.

[a] GI_{50}: 50% growth inhibition.

[b] SI: Selectivity index (GI_{50} MRC-5/GI_{50} cancer cell line).

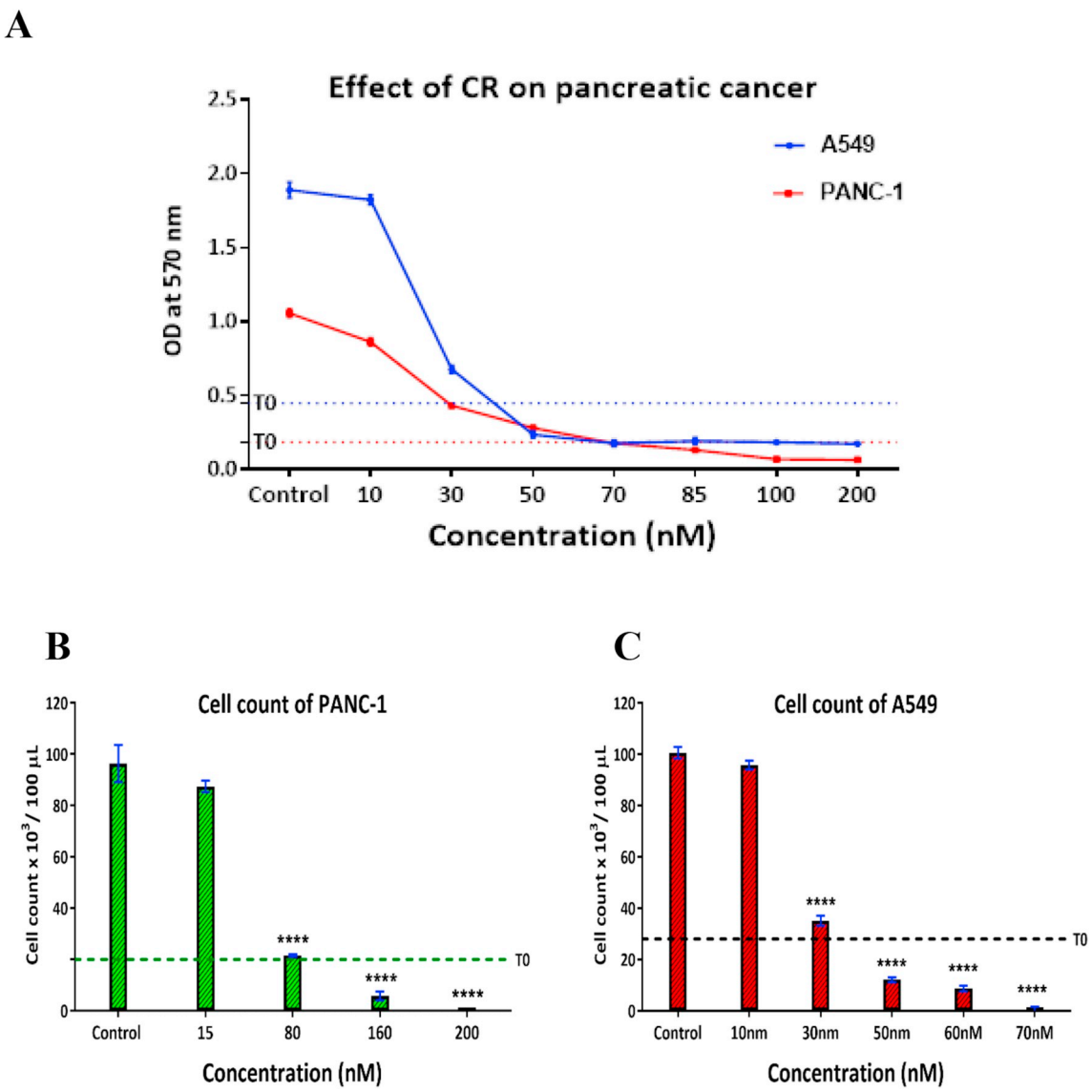

Fig. 2. Growth inhibitory effects and cell count of CR.(**A**) Representative graph showing growth inhibitory effects of CR on PANC-1 and A549 cells. Cells were seeded at a density of 3×10^3 cells/well in 96-well plates and incubated for 72 h (n = 6; ≥3 trials). Effects of CR on PANC-1 (**B**) and A549 (**C**) cell numbers. Cells (2×10^4 cells/well) were seeded in 6-well plates and incubated overnight before treatment with CR (10–200 nM; 72 h). Cells were harvested and counted by haemocytometer (n = 2; ≥3 trials).

(HK-1) and 130.2 nM (SKBR-3). Interestingly, CR demonstrated 315.64–1838.92-fold and 26–155.5-fold selectivity towards cancer cells compared to MRC-5 non-transformed fibroblasts (GI_{50} = 41.10 µM) and normal nasopharyngeal NP-69 cells (GI_{50} > 3.46 µM) respectively (Table 2).

To validate MTT assay results, cell counts were performed following 72 h exposure of PANC-1 and A549 cells to CR. Dose-dependent reductions in cell numbers were particularly evident between 17 nM and 200 nM in PANC-1 and 10 nM–70 nM in A549 cells. Nanomolar CR concentrations caused cytotoxicity in both cell lines as significantly fewer cell numbers were counted than originally seeded (Fig. 2 B and C; $p < 0.0001$).

3.4. CR inhibited cancer colony formation

After brief (24 h) exposure to CR, colony formation was significantly inhibited in human-derived cancer cells (Fig. 3A and B). At 1 × and 2 × GI_{50} respectively, CR inhibited colony formation in: HT-29 (35%, 74%); HCT-116 (85%, 99.3%); MIA PaCa-2 (79%, 100%); HK-1 (70%, 100%); A549 (95%, 100%); MDA-MB-468 (71%, 84%); MDA-MB-231 (51%, 89%); MCF-7 (76%, 93%); PANC-1 (70%, 97.3%) cells (Fig. 3A and C). The clonogenic assay corroborated anticancer potency and cytotoxicity of CR. Although differences in sensitivity to CR between cell lines were detected, colony formation was significantly inhibited ($p < 0.0001$).

3.5. CR inhibited cancer cell migration

Tumour cell migration plays a crucial role in metastasis [33]. A wound healing assay was implemented to investigate the effect of CR on the migration of PANC-1, MDA-MB-468 and A549 cells (Fig. 4). Compared to vehicle control, CR significantly and dose-dependently inhibited migration of PANC-1, MDA-MB-468 and A549 cells. Untreated PANC-1 and A549 controls showed 100% closure of the wound within 48 h. In MDA-MB-468 control cells, migration progressed more slowly and wound closure was estimated to have reached 93% 48 h. CR exhibited 4- to 26-fold inhibition of wound healing in all three cell lines at 2 × GI_{50} concentration after 48 h (Fig. 4).

Table 2
Effect of CR on the growth of human-derived cancer cells.

Cells	Breast carcinoma				Colon carcinoma		
	MCF-7	MDA-MB-231	MDA-MB-468	SKBR-3	HCT-116	HT29	VR-HCT-116
Mean GI_{50}[a] ± SD (nM)	28.2 ± 2.80	42.8 ± 5.26	73.7 ± 0.69	130.2 ± 6.14	60.1 ± 1.27	55.1 ± 2.75	69.6 ± 1.03
SI[b] compared to the **MRC-5** cells	1457	967	557.36	315	683	745	590
SI[b] compared to the **NP-69** cells	122.9	81.02	47	26.6	57.7	62.9	49.8

Cells	Pancreatic carcinoma		Nasopharyngeal carcinoma	Small lung carcinoma	Liver carcinoma	Human foetal lung fibroblast cells	Normal nasopharyngeal epithelial cells
	Panc-1	MIA PaCa-2	HK-1	A549	HepG2	MRC-5	NP-69
Mean GI_{50}[a] ± SD (nM)	23.6 ± 3.62	90 ± 2.66	22.3 ± 0.67	45.8 ± 1.00	69.3 ± 1.43	41100 ± 1560	> 3467
SI[b] compared to the **MRC-5** cells	1740	456	1838	896	592		
SI[b] compared to the **NP-69** cells	146.9	38.5	155.5	75.7	50		

Mean ± SD GI_{50} values were determined by MTT assays following 72 h exposure of cells to test CR (n = 4) and expressed as a mean ± SD of ≥3 independent trials.

[a] GI_{50}: 50% growth inhibition.

[b] SI: Selectivity index (GI_{50} of MRC-5 or NP-69 cells/GI_{50} of cancer cell line).

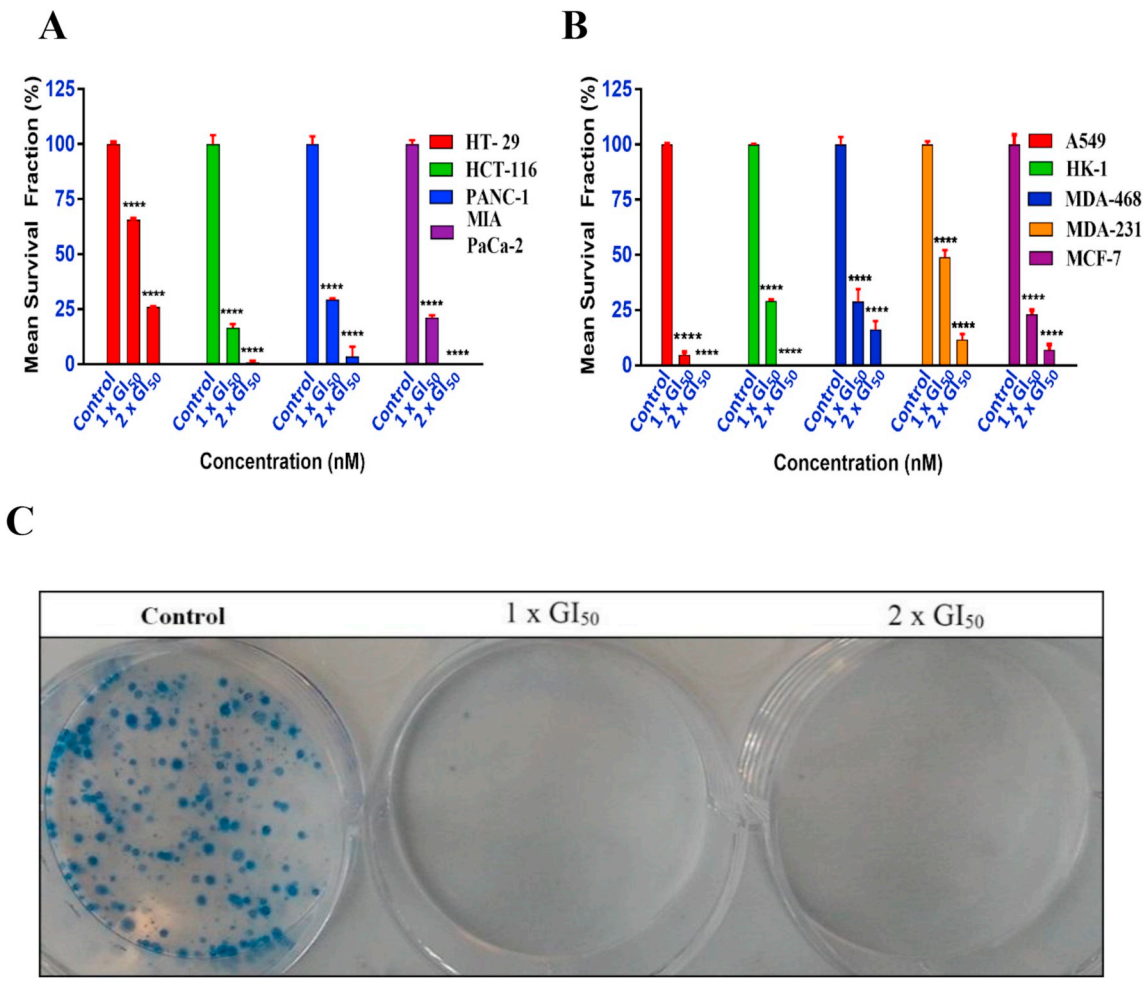

Fig. 3. Mean survival fraction (%) of CR treated cells.(**A** and **B**) Mean ± SEM survival fraction (%) of treated cells as a percentage of the control population for A549, MDA-MB-468, MDA-MB-231, PANC-1, HK-1, HCT-116, HT-29, MCF-7 and MIA PaCa-2 cells. CR caused a significant reduction in colony formation (****$p < 0.0001$, $n = 2$ for each of the 3 trials). (**C**) Representative photograph showing the effect of CR on PANC-1 colony formation at control, 1 × GI_{50} and 2 × GI_{50}.

3.6. Generation of DNA double strand breaks

γ-H2A.X is considered a DNA double-strand break (DSB) marker, which can be quantified to assess DNA damage [24]. The induction of DNA damage by CR was assessed following analyses of the number of cells expressing γ-H2A.X detected by flow cytometry. As demonstrated in Fig. 5, CR significantly increased γ-H2A.X foci in PANC-1, MBA-MB-468 and A549 cells by 9-, 2.6- and 12-fold respectively, relative to the control. The positive control etoposide caused similar γ- H2A.X elevation in PANC-1 (6.18-fold), MDA-MB-468 (2.7-fold) and A549 (7.5-fold).

3.7. Cell cycle analysis

Results shown so far suggest that CR inhibits cancer cell growth and viability following infliction of cancer cell DNA damage. Based on these observations, we investigated the effect of CR on cell cycle perturbation by flow cytometry. Cells were exposed to CR (1 × GI_{50} and 2 × GI_{50}) for 24, 48 and 72 h. Time- and dose-dependent accumulation of events in G2/M phases were sustained in PANC-1, MDA-MB-468 and A549 cell lines, with significant G2/M cell cycle arrest observed following 24, 48 and 72 h exposure at 1 × GI_{50} and 2 × GI_{50} (Fig. 6). CR induced the highest accumulation of events in G2/M phases after 72 h exposure: 56.8%, 43% and 33.5% in MDA-MB-468, PANC-1 and A549 populations respectively. In Supplementary Fig. S3, the stark dose-dependent accumulation of HCT 116 events in the G2/M cell cycle phase is evident. Accumulation of A549 events in G1 at 1 × GI_{50} and 2 × GI_{50} was observed after 48 h exposure accompanied by significant elevation of cells in the sub-G0/G1 phase. One of the most sensitive cell lines (inferred by MTT assays), PANC-1 revealed that G2/M cell cycle arrest was accompanied by a significant pre-G1 population at 2 × GI_{50} following 72 h exposure, indicative of apoptosis. Cell cycle profiles are shown in Supplementary Fig. S2.

3.8. CR induces apoptosis in cancer cells

Annexin-V/PI evaluation of apoptosis in conjunction with caspase 3/7 activation assays were performed to investigate the apoptosis-inducing properties of CR in PANC-1, MDA-MB-468 and A549 cell lines exposed to CR (1 and 2 × GI_{50}; 24, 48 and 72 h). Apoptotic populations were confirmed by dual annexin V-FITC/PI staining (corresponding scatter plots are shown in Supplementary Fig. S4). CR evoked profound time-dependent apoptosis. PANC-1 cells showed significant early (A+/PI-) apoptosis at 1 × GI_{50} (48 and 72 h) and 2 × GI_{50} at 24, 48 and 72 h exposure ($p < 0.05$, $p < 0.01$ and $p < 0.0001$, respectively); cells appeared more resistant to late (A+/PI+) apoptosis at both 1 × GI_{50} and 2 × GI_{50} (Fig. 7A), possibly indicating slower apoptosis onset. However, CR induced significant early MDA-MB-468 apoptosis at 1 × GI_{50} and 2 × GI_{50} following 48 and 72 h exposure ($p < 0.0001$); late MDA-MB-468 apoptosis was observed at 1 × GI_{50} (72 h) and 2 × GI_{50} at both 48 and 72 h exposure (Fig. 7B). Similarly, A549 revealed significant early apoptosis following CR treatment at 1 × and

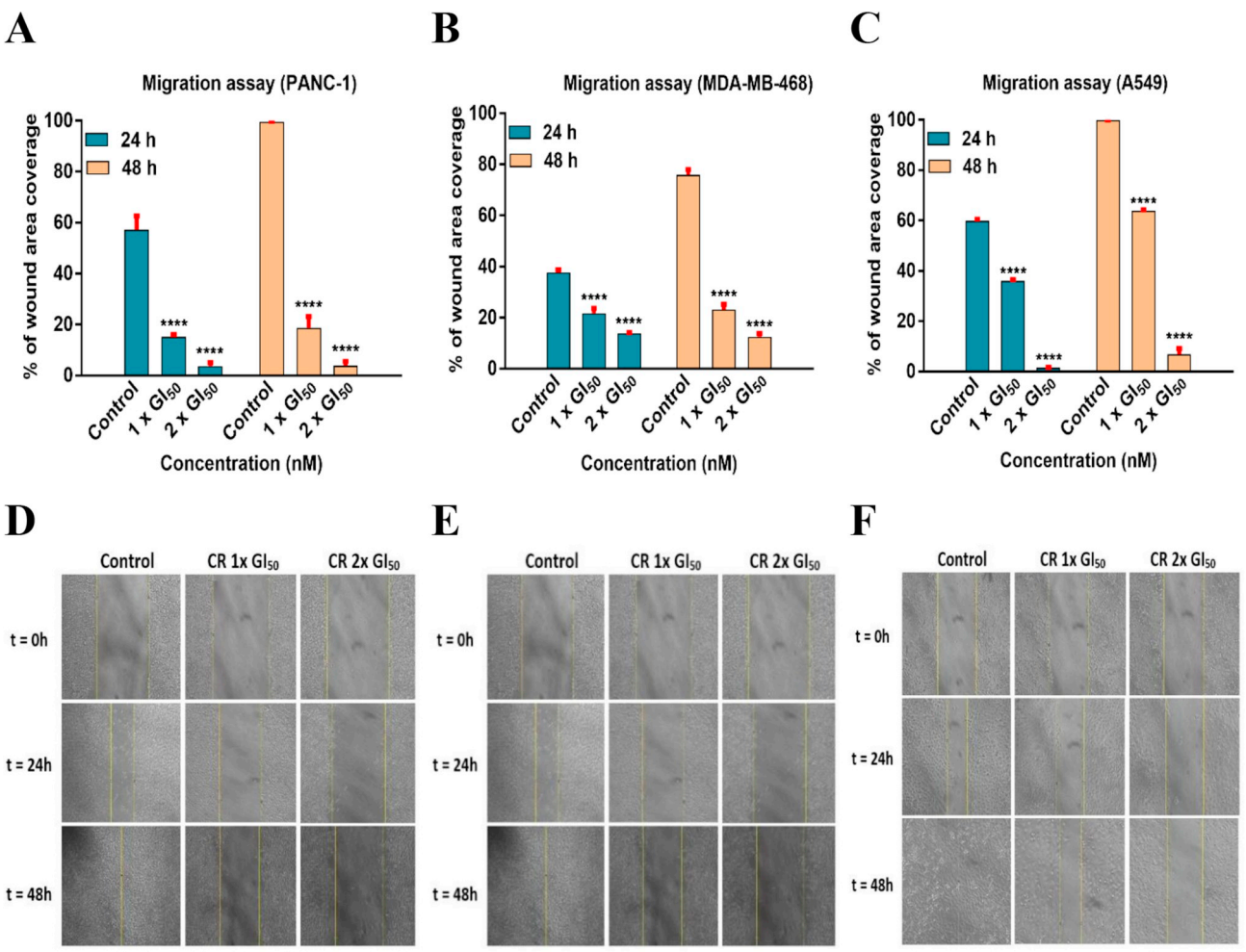

Fig. 4. Effects of CR on cell migration in PANC-1, MDA-MB-468 and A549 cells. (**A-C**) CR inhibited migration of PANC-1, MDA-MB-468 and A549 cells; wounds were evaluated after 24 and 48 h exposure to CR at 1 × and 2 × GI_{50} values. CR induced significant (****p < 0.0001) inhibition of cell migration compared to the control with medium only. Mean ± SD ≥ 3 independent trials (n = 2). (**D-F**) Representative microscopic images from one of the experiments demonstrating potent inhibition of cell migration of PANC-1, MDA-MB-468 and A549 cells by CR (1 × GI_{50} and 2 × GI_{50}). Image J was used to measure the surface area of the wound.

2 × GI_{50} after 48 and 72 h treatment ($p < 0.001$ and $p < 0.0001$, respectively), and late apoptosis at 2 × GI_{50} only after 48 and 72 h exposure (Fig. 7C). The highest percentage apoptosis at 2 × GI_{50} was observed in A549 populations after 72 h exposure to CR (~37%), compared to MDA-MB-468 (~28%) and PANC-1 (~23%).

Induction of caspase-3/7 activity was measured in PANC-1, MDA-MB-468 and A549 cells after 24 h exposure to either CR (1 × GI_{50} and 2 × GI_{50}) or vincristine (10 nM; Fig. 7D). CR significantly increased caspase 3/7 activity in all three cell lines compared to the control ($p < 0.0001$). In PANC-1, MDA-MB-468 and A549 populations, 1 × GI_{50} and 2 × GI_{50} CR concentrations enhanced caspase activity by 170% and 322%; 190% and 439%; 133% and 194% respectively. Vincristine also increased caspase activity in PANC-1 (115%), MDA-MB-468 (197%) and A549 (190%) cells.

3.9. CR induces ROS production in cancer cells

ROS production was measured in PANC-1, MDA-MB-468 and A549 cells following 24 h treatment with CR (1 × GI_{50} and 2 × GI_{50}) or vincristine (10 nM) (Fig. 8). At 1 × GI_{50} CR significantly ($p < 0.001$) increased ROS production to 147%, 156% and 155% compared to controls in PANC-1, MDA-MB-468 and A549 cells, respectively; at 2 × GI_{50} CR, ROS generation increased to 165%, 305% and 190% of controls in PANC-1, MDA-MB-468 and A549 cells, respectively.

3.10. CR treatment leads to alterations in protein expression

Western blot was used to investigate changes in protein expression and activation of signal transduction cascades known to possess roles in apoptosis, mitosis and cell survival. Lysates of PANC-1, MDA-MB-468 and A549 cells following 24 and 72 h exposure of cells to 2 × GI_{50} CR were prepared. Significant time-dependent elevation in cleaved PARP accompanied a reduction in expression of anti-apoptotic/pro-survival proteins Mcl-1 and Bcl-2 compared to the untreated control (Fig. 9A–E), consistent with apoptosis-induction. Significant down-regulation of PLK1 was observed after exposure of cells to CR (24 and 72 h; $p < 0.0001$) (Fig. 9A and F).

3.11. CR modulates signalling through PI3K/AKT/mTOR pathways

The PI3K-AKT-mTOR signalling pathway plays an essential role in tumourigenesis including cancer cell survival, proliferation and protein translation [34]. Therefore, we examined whether CR impacts activation of this pathway in PANC-1, MDA-MB-468 and A549 cancer cells. Cultures of all three cancer cell lines were treated with CR at 2 × GI_{50} for 24 and 72 h. Time-dependent attenuation of PI3K, AKT, and 4EBP1 phosphorylation was observed, whereas total PI3K, AKT and 4EBP1 protein expression remained unchanged (Fig. 10A–D). The oncogenic transcription factor STAT3 is commonly constitutively activated in tumours and tumour-derived cell lines [35]. Our results also revealed that

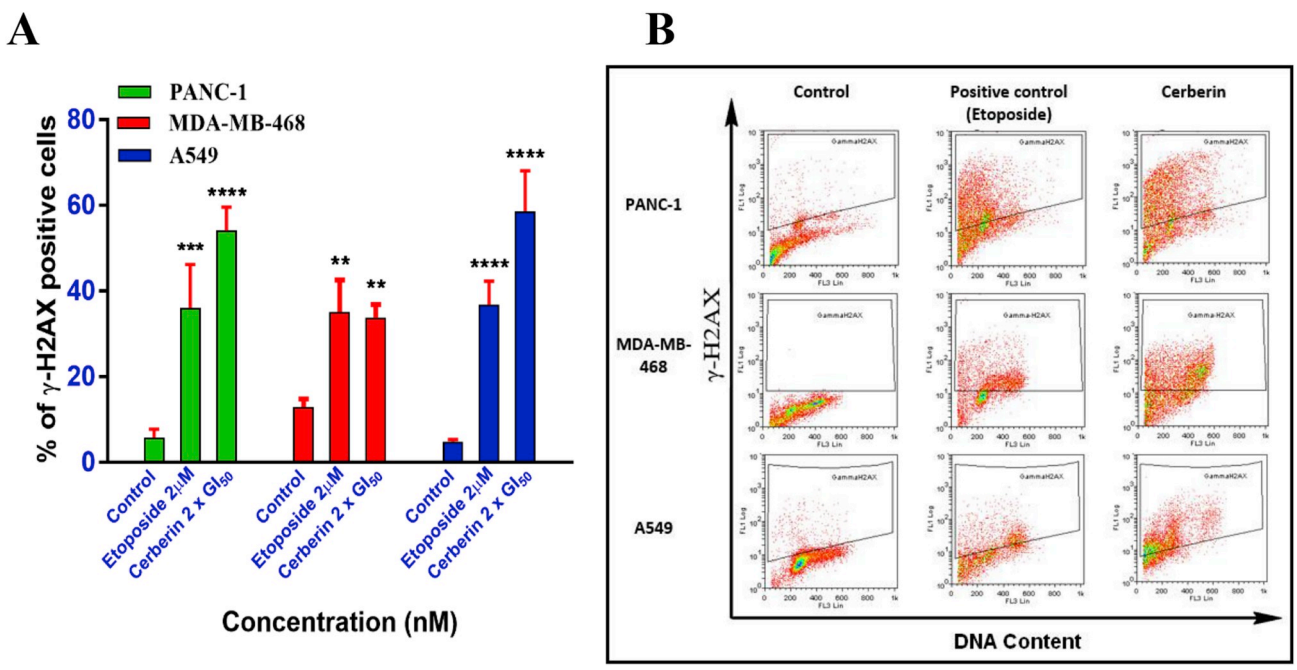

Fig. 5. CR-induced DNA DSBs in PANC-1, MDA-MB-468 and A549 cells. (**A**) CR (2 × GI_{50} value) induced DNA DSBs in PANC-1, MDA-MB-468 and A549 cells after 24 h exposure. Etoposide (2 μM) was used as a positive control as it is a known DNA damaging agent. CR caused a significant increase in γ-H2A.X formation (**p < 0.01, ***p < 0.001 and ****p < 0.0001 vs untreated control). (**B**) Representative γH2A.X dot plots from an independent trial illustrating induction of DNA DSBs in PANC-1, MDA-MB-468 and A549 after 24 h of CR treatment. Experiments were repeated at least 3 times (n = 2).

CR downregulates STAT3 phosphorylation with no changes in total STAT3 expression (Fig. 10 A and E). The mammalian target of rapamycin (mTOR) is also commonly activated in cancer and regulates cell proliferation, metabolism, survival and metastasis. Therefore, we investigated the effect of CR on mTOR phosphorylation. Interestingly, CR downregulated phosphorylation of mTOR (*p*-mTOR) (Fig. 10F and G), correlating with PI3K/AKT/mTOR inhibition. Again, no significant changes in total mTOR protein were observed.

3.12. CR causes severe disruption in cytoskeletal architecture

G2/M arrest revealed during cell cycle analyses may be indicative of tubulin/microtubule disruption, therefore, following 24 h exposure to vehicle alone (control), CR (1 × GI_{50}) or vincristine (10 nM), MDA-MB-468 cells were immunostained and prepared for inspection by confocal microscopy. To investigate the morphological changes in cytoskeletal, chromosomal and cellular characteristics, tubulin and DNA were stained, and CR-treated cells were compared to those exposed to the vehicle alone or vincristine. Fig. 11A–D represent MDA-MB-468 control cells. Cells treated with the microtubule depolymerising agent vincristine (10 nM; Fig. 11E–H) revealed irregular chromosomal separation (Fig. 11E and F), nuclear membrane disruption, microtubule network disruption and uneven cell division, consistent with its mechanism of action; additionally, chromatin condensation, heralding apoptosis, was detected (Fig. 11G and H). Similar to vincristine, CR caused tubulin network disruption leading to improper chromosome segregation, accompanied by aneuploidy and multinucleation (Fig. 11J and K). Uneven cell division was also detected in CR-treated MDA-MB-468 cells (Fig. 11L–P). CR treatment also evoked nuclear fragmentation, chromatin lunate morphology and condensation accompanied by severe membrane blebbing (Fig. 11M–P), characteristics associated with apoptosis.

3.13. In silico pharmacokinetic properties of CR

The pharmacokinetic (PK) properties of CR were simulated in mice, as rodents are the most likely first species tested in preclinical evaluation (Fig. 12, Table 3). GastroPlus™ is a powerful *in silico* prediction tool in the area of biopharmaceutics and pharmacokinetics with the ability to provide useful information and guidelines prior to expensive and time-consuming *in vivo* experiments [19,36–38]. Plasma concentration-time profiles of CR following various routes of administration were simulated to predict the levels of systemic exposure for each route (Fig. 12 A). CR was predicted to be rapidly eliminated with an elimination half-life of 1.6 h following intravenous administration. Following oral administration, CR was predicted to be rapidly absorbed with maximum concentration achieved at 0.4 h with relatively high bioavailability (61.2%). Subcutaneous absorption was predicted to show slower but almost complete absorption with 96.6% bioavailability (Table 3).

Simulations were performed to predict the dose range needed in preclinical development of CR. As it is the unbound drug that exerts its pharmacological effect [39], unbound concentration profiles of CR in plasma following oral administration at a range of doses were simulated (Fig. 12 B). The lowest (HK-1) and the highest (SKBR-3) GI_{50} values obtained for cancer cell lines were also plotted to visualise effective dose range. The modelling suggested that doses between 1 and 10 mg/kg CR would exert anti-tumour activity in preclinical murine models. A dose of 100 mg/kg was predicted to cause possible issues with CR absorption, showing irregular profiles. As GastroPlus™ employs the ACAT model for oral absorption, the amount (%) of CR predicted to be absorbed in each compartment of the GI tract is also shown (Fig. 12C). CR was predicted to be absorbed mostly at the proximal region of the GI tract. Simulated PK results provide a useful guideline for further preclinical development of CR as a promising anticancer therapy.

4. Discussion

Throughout history, it has been recognised that Nature provides a rich source of potential medicinal agents – molecules possessing structural complexity and diversity able to perturb molecular mechanisms critical to disease pathogenesis. Pursuit of natural product

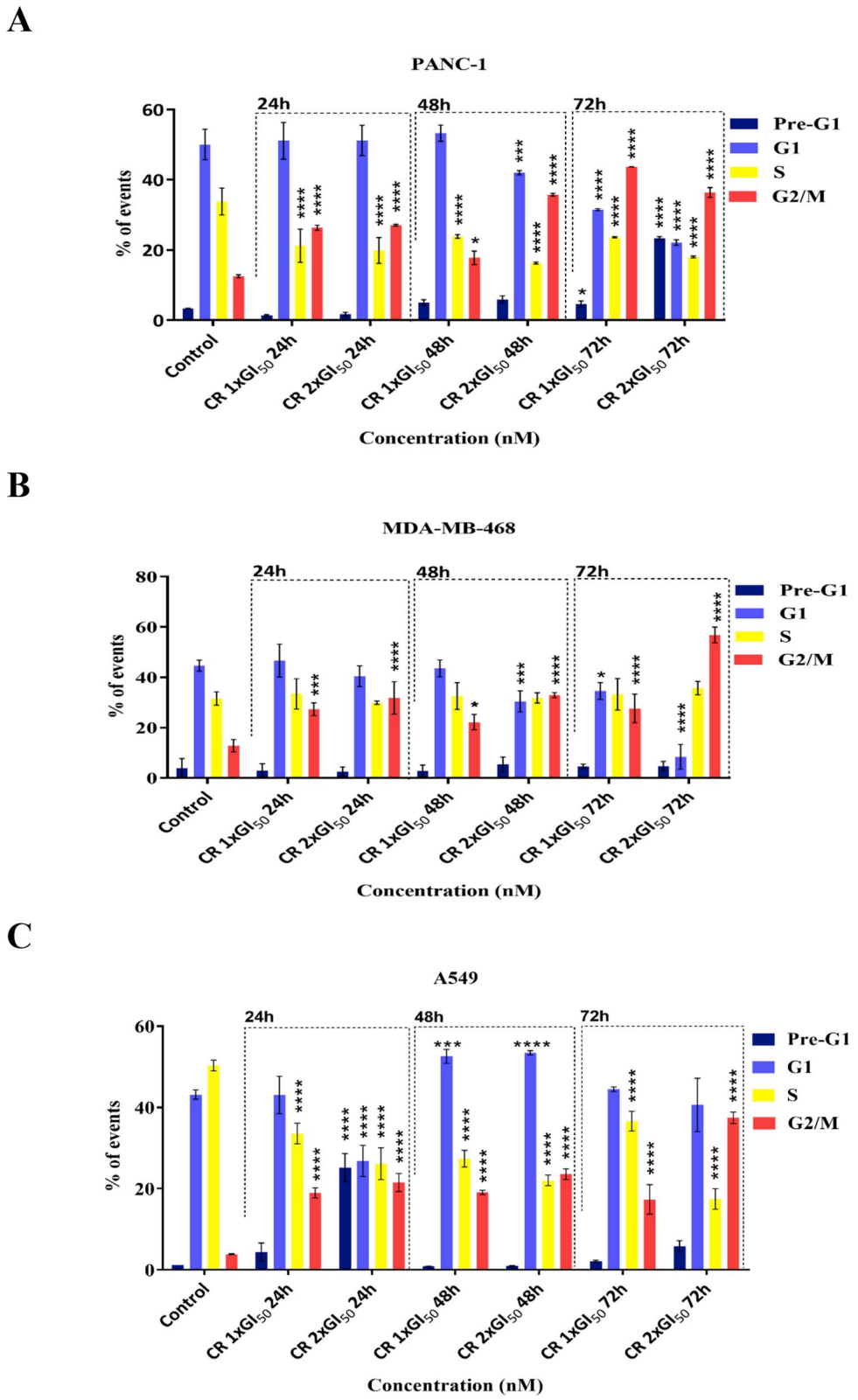

Fig. 6. Effect of CR on cell cycle in PANC-1, MDA-MB-468 and A549 cells. PANC-1 (**A**), MDA -MB-468 (**B**) and A549 (**C**) cells were treated with 1 × GI_{50} and 2 × GI_{50} CR for 24, 48 and 72 h. CR evoked significant arrest in the G2/M phase (*p < 0.01, ***p < 0.001 and ****p < 0.0001; experiments were repeated ≥3 times, n = 2).

drug discovery is critical to identify novel compounds able to combat intractable and drug-resistant diseases before habitat loss leads to extinction.

Recent research has focussed on CGs such as ouabain, oleandrin, digoxin, as putative anticancer agents [40]. These CGs exert potent *in vitro* anticancer activity and are non-toxic towards normal cells [41]. Epidemiological studies have shown that patients receiving CG treatment for heart failure appear protected from certain cancer types

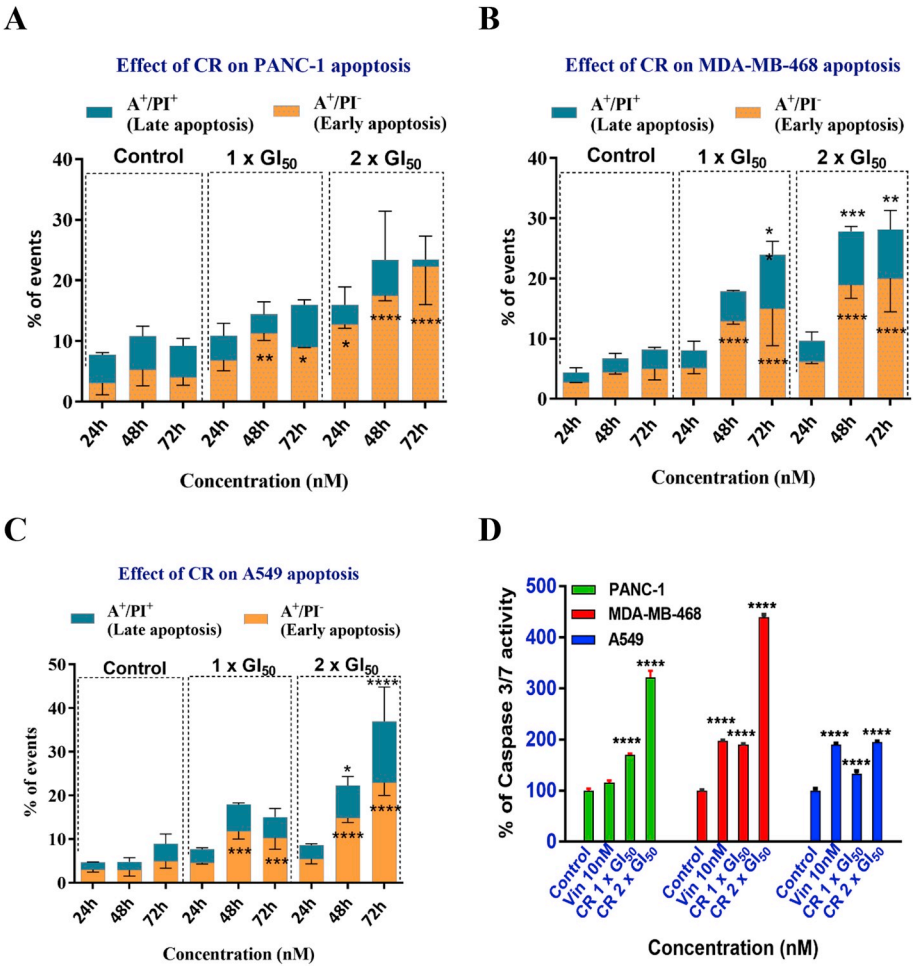

Fig. 7. Effects of CR on PANC-1 (A), MDA-MB-468 (B) and A549 (C) apoptosis. Cells were treated with 1 × and 2 × GI_{50} CR for 24, 48 and 72 h. Annexin-V/PI apoptosis assays were performed to determine the percentage of apoptotic cells. Total apoptosis comprises early apoptotic (annexin V-positive and PI negative) and late apoptotic (annexin V-positive and PI positive) populations. Mean ± SEM ≥3 independent trials (n = 2 per trial; 10,000 events were analysed per sample). (**D**) Effect of CR on caspase 3/7 activity in PANC-1, MDA-MB-468 and A549 cells after 24 h exposure to 1 × GI_{50} and 2 × GI_{50}. Mean ± SEM ≥3 independent trials (n = 2 per trial). CR caused significant increase in caspase 3/7 activity (*p < 0.05, **p < 0.01, ***p < 0.001 and ****p < 0.0001; experiments were repeated ≥3 times, n = 2).

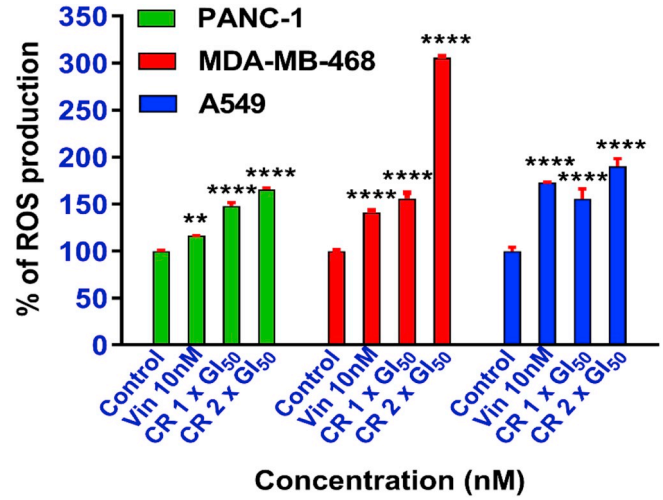

Fig. 8. CR induced significant levels of ROS production in PANC-1, MDA-MB-468 and A549 cells. Cells were treated with CR (1 × GI_{50} or 2 × GI_{50}) or vincristine (10 nM). Mean ± SD ROS generation is depicted as a percentage of untreated control (***p < 0.001 and ****p < 0.0001, n = 2 for each of 3 independent trials).

[42,43]; three CGs have progressed to clinical evaluation as anticancer therapies [46].

In this study we have isolated cerberin (CR), a cardenolide cardiac glycoside (CG) and shown that it evokes significant, potent (nanomolar), broad-spectrum and selective (> 300-fold) anticancer activity. Herein, we report our efforts to clarify the nature of *in vitro* antitumour activity and elucidate molecular mechanisms of action of CR.

MTT and cell count assays revealed the potent growth inhibitory activity of CR; inhibition of carcinoma colony formation indicated that cells were either killed, or lost the proliferative ability to form progeny colonies. Estimated GI_{50} values (calculated from MTT assays) were adopted in subsequent assays designed to interrogate molecular targets of CR.

Flow cytometric analyses of CR-treated PANC-1, MDA-MB-468 and A549 cells demonstrated significant G2/M cell cycle arrest, which may indicate interrupted mitoses and cytoskeletal protein targets. Indeed, confocal microscopy revealed tubulin network disorder, multipolar spindles, misaligned chromosomes and multinucleation – clear evidence of cytoskeletal architecture disruption. Microtubule disruption is likely to impact cell migration, a key component of invasion and metastasis – a fundamental cancer hallmark [48] and important target for intervention in anticancer drug discovery [47]. It was shown that CR exhibited significant anti-migratory activity in the same cancer cell lines (PANC-1, MDA-MB-468, A549). Polo-like kinase 1 (PLK1) possesses key roles leading to promotion of mitosis including modulation of cdc2 activation, chromosome segregation and formation of bipolar spindles. Enhanced levels of PLK1, a recognised oncogene and validated anticancer drug target [52], are evident in malignant compared to normal tissue [19,53]. CR caused significant time-dependent down-regulation of PLK1. Similarly, the CG bufalin supressed PLK1 protein expression, delaying entry of cells into prophase, arresting cell cycle, ultimately leading to apoptosis [53].

CR is known to inhibit NA^+/K^+-ATPase (NKA), reducing NA^+ and elevating Ca^{2+} intracellular levels, impacting signal transduction

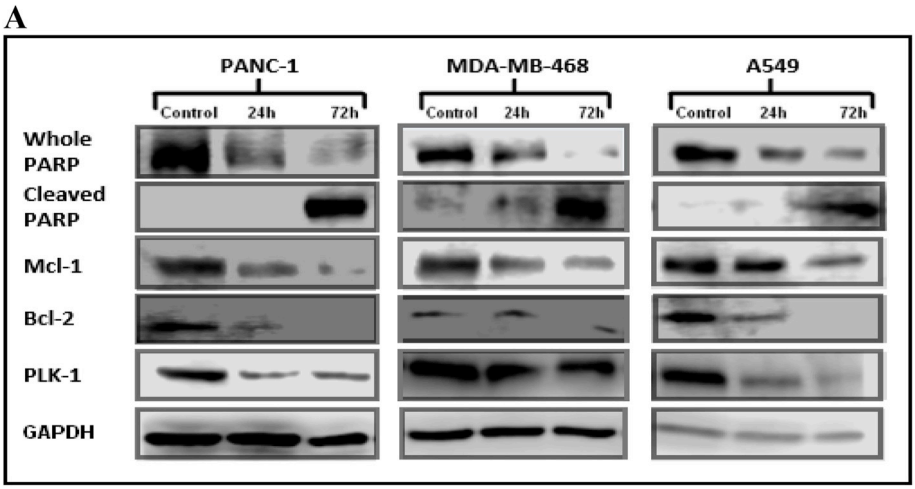

Fig. 9. (**A**) Representative Western blots of lysates prepared from PANC-1, MDA-468 and A549 cells exposed to 2 × GI_{50} CR for 24 or 72 h; extracted proteins were separated by SDS-PAGE and analysed using antibodies to detect whole and cleaved PARP, Mcl-1, Bcl-2, PLK-1 and housekeeping gene GAPDH. (**B-F**) Collated densitometric measurement of protein expression levels; PARP cleavage was observed at 2 × GI_{50} and was accompanied by a time-dependent decrease in Mcl-1 and Bcl-2. PLK-1 downregulation was observed in all three cell lines. GAPDH was used as an internal loading control. Data represent the mean ± SD of 3 independent experiments (ANOVA followed by Dunnett's test). Significance is reported as: *P < 0.05, **P < 0.01, ***P < 0.001 and ****P < 0.0001 compared to controls.

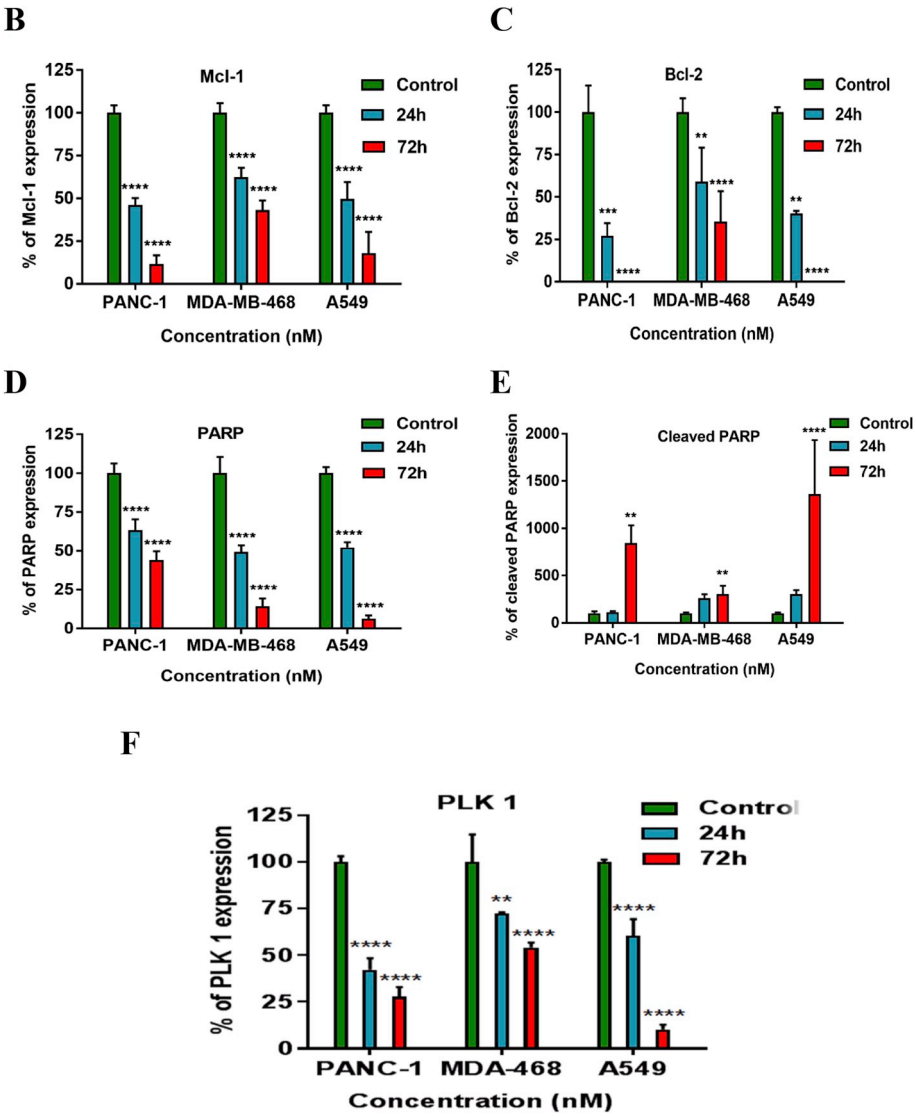

Fig. 9. (*continued*)

cascades and modulating key cellular functions including proliferation and apoptosis [43]. NKA also interacts with signalling proteins (PKC, PKA, PI3K, MAPK, EGFR; known as the signalosome), inspiring further interest in CGs as anticancer agents [44,45].

With this knowledge in mind, the effects of CR on transcription factor c-Myc expression (reported in SI), PI3K-AKT-mTOR and signal transducer and activator of transcription 3 (STAT 3) activation were interrogated by western blot. Down-regulation of c-Myc was evident after treatment of cells with CR; c-Myc depletion is known to negatively impact cancer cell survival [54]. PI3K pathway activation similarly has important consequences on cancer cell survival, and is pivotal for protein translation and angiogenesis. Mutations leading to PI3K pathway deregulation promote tumourigenesis [55]. The eukaryotic translation initiation factor 4E-binding protein 1 (4E-BP1) is regulated by PI3K, AKT and mTOR signalling; interestingly, Bcl-2 is regulated by 4E-BP1. In MDA-MB-468 and A549 cells, CR significantly inhibited mTOR phosphorylation. For sustainable, long-term benefit, dual mTOR and AKT/PI3K inhibitors may need to be employed to thwart cancer recurrence or emergence of drug-resistance [55]; herein, we demonstrate down-regulation of PI3K, AKT and mTOR phosphorylation by CR. 4EBP1, a repressor of protein translation, is the first downstream substrate of mTOR; phosphorylated 4EBP1 is associated with tumour progression and poor prognosis [57]. CR also downregulated phosphorylation of 4EBP1. Finally, CR significantly supressed STAT 3 phosphorylation in the 3 cell lines examined (PANC-1, MDA-MB-468 and A549) following treatment with CR (24 h; 48 h); STAT 3 has

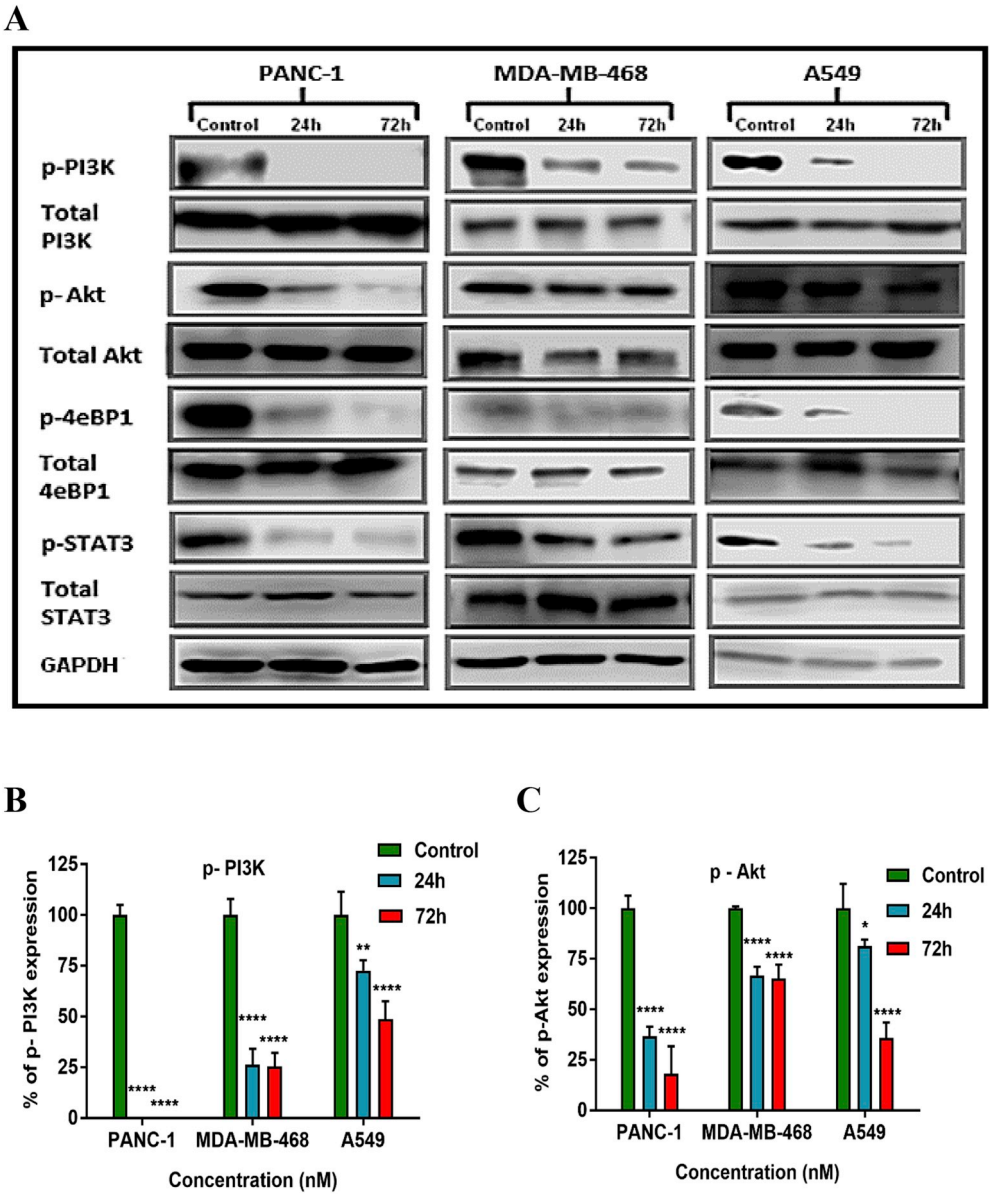

Fig. 10. (A) Representative Western blots of lysates prepared from PANC-1, MDA-468 and A549 cells treated with 2 × GI_{50} CR for 24 or 72 h; extracted proteins were separated by SDS-PAGE and analysed using antibodies to detect total and phosphorylated PI3K (p-PI3K), AKT (*p*-AKT), 4EBP1 (p-4EBP1), STAT3 (p-STAT3) and housekeeping gene GAPDH. (**B-E**) Collated densitometric analyses of protein expression levels; time-dependent downregulation of p-PI3K, *p*-AKT, p-4eBP1 and p-STAT3 were observed at 2 × GI_{50} CR after 24 and 72 h treatment; no significant changes occurred in total AKT, 4eBP1, PI3K and STAT3 protein expression. GAPDH was used as an internal loading control. Data represent the mean ± SD of 3 independent experiments (ANOVA followed by Dunnett's test). Significance is reported as: *P < 0.05, **P < 0.01, ***P < 0.001 and ****P < 0.0001 compared to controls. (**F**) Western blot analyses of *p*-mTOR in MDA-MB-468 and A549 cells. Cells were treated with 2 × GI_{50} CR for 24 and 72 h. (**G**) Collated densitometric measurement of protein expression levels; time-dependent downregulation of *p*-mTOR was observed at 2 × GI_{50}; data are means ± SD of 3 independent experiments (ANOVA followed by Dunnett's test). Significance: ***P < 0.001 and ****P < 0.0001 compared to controls.

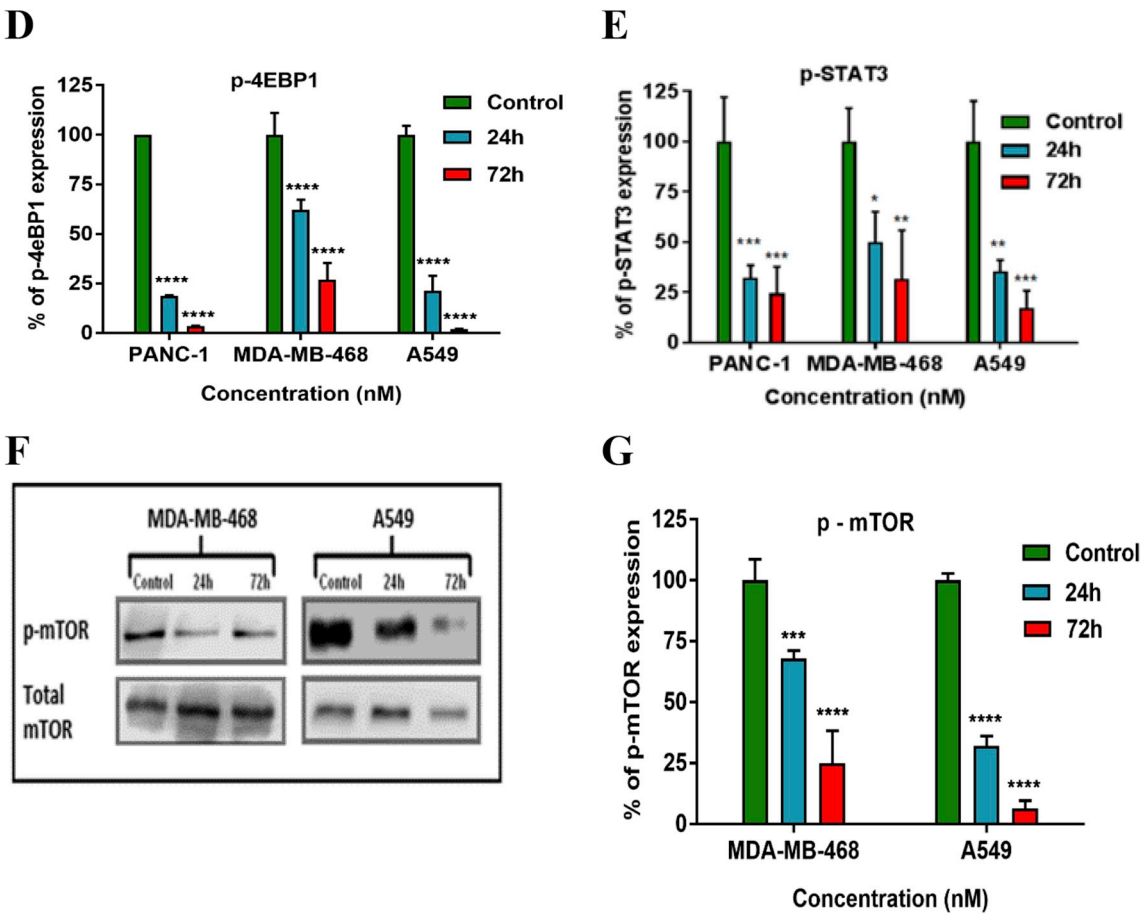

Fig. 10. (*continued*)

regulatory roles in diverse cellular functions including metastasis, angiogenesis, malignant immune-suppression and apoptosis and its constitutive activation leads to poor cancer prognosis [56].

This study therefore demonstrates that CR possesses anti-oncogenic properties concurrently perturbing multiple molecular targets pertinent to tumourigenesis. That the ultimate consequence of CR treatment is cancer cell apoptosis has been shown by flow cytometry, caspase activation, confocal microscopy and western blot.

During early apoptosis, cellular membrane integrity is lost exposing phosphatidylserine (PS) on the outer membrane leaflet. Annexin V-FITC binds with high affinity to PS, a property that has been extensively exploited to quantify early apoptosis [50]. As apoptosis progresses, membrane integrity is lost allowing cells to stain positive for PI. Activation of caspases is a hallmark of apoptosis, specifically executioner caspase 3 [23, 51]. Therefore, annexin V-FITC/PI flow cytometry detection and caspase 3/7 activation assays were adopted, and confirmed emergence of PANC-1, MDA-MB-468 and A549 apoptotic populations. Consistent with cell cycle arrest and the appearance of DNA damage, time- and dose-dependent annexin V-positive (early apoptotic) populations were evident in all 3 cell lines; whereas, significant late apoptosis was observed in MDA-MB-468 and A549 cells (48 h; 72 h exposure CR).Clear induction of caspase 3/7 activity was demonstrated in all 3 cell lines. Confocal microscopy revealed evidence of apoptotic characteristics such as chromatin condensation, DNA fragmentation and membrane blebbing [9,49]. Concomitantly, cleaved PARP, and down-regulation of anti-apoptotic proteins Bcl-2 and Mcl-1 were detected. Cancers commonly express elevated levels of oncogenic Bcl-2 protein family members and their down-regulation modulates cancer cell survival.

In order for promising experimental anticancer agents to progress through *in vivo* and clinical evaluation, drug metabolism and pharmacokinetic studies are necessary to determine agent bioavailability. Gastroplus™ is a powerful preclinical tool used in drug discovery: results of *in silico* biopharmaceutical evaluation inferred that CR concentrations able to evoke antitumour activity and perturb molecular targets and signal cascades driving tumourigenesis were achievable following oral administration of CR doses between 1 and 10 mg/kg. Oral (self) administration is known to improve patient adherence and reduces costs associated with in-patient treatment [58].

In summary, we have shown that CR elicits potent and selective anticancer activity, significantly inhibiting cancer cell proliferation, migration and colony survival in human-derived pancreatic, triple negative breast and non-small cell lung cancer cell lines. Profound G2/M cell cycle arrest and disruption of cytoskeletal architecture were demonstrated. Intriguingly, CR inhibited molecular targets portending potential to perturb multiple cancer hallmarks: CR suppressed PI3K/AKT/mTOR and STAT 3 signal transduction and down-regulated PLK 1, c-Myc, Bcl-2 and Mcl-1 expression. CR significantly increased ROS production and caused DNA DSBs, ultimately inducing apoptosis. Finally, we predict that CR may be administered at doses that provide efficacious anticancer plasma concentrations, therefore, further preclinical evaluation of CR is justified.

Conflicts of interest

The authors have no conflicts of interest.

Acknowledgements

GastroPlus™ software was kindly provided by Simulations Plus, Inc, Lancaster, California, USA.

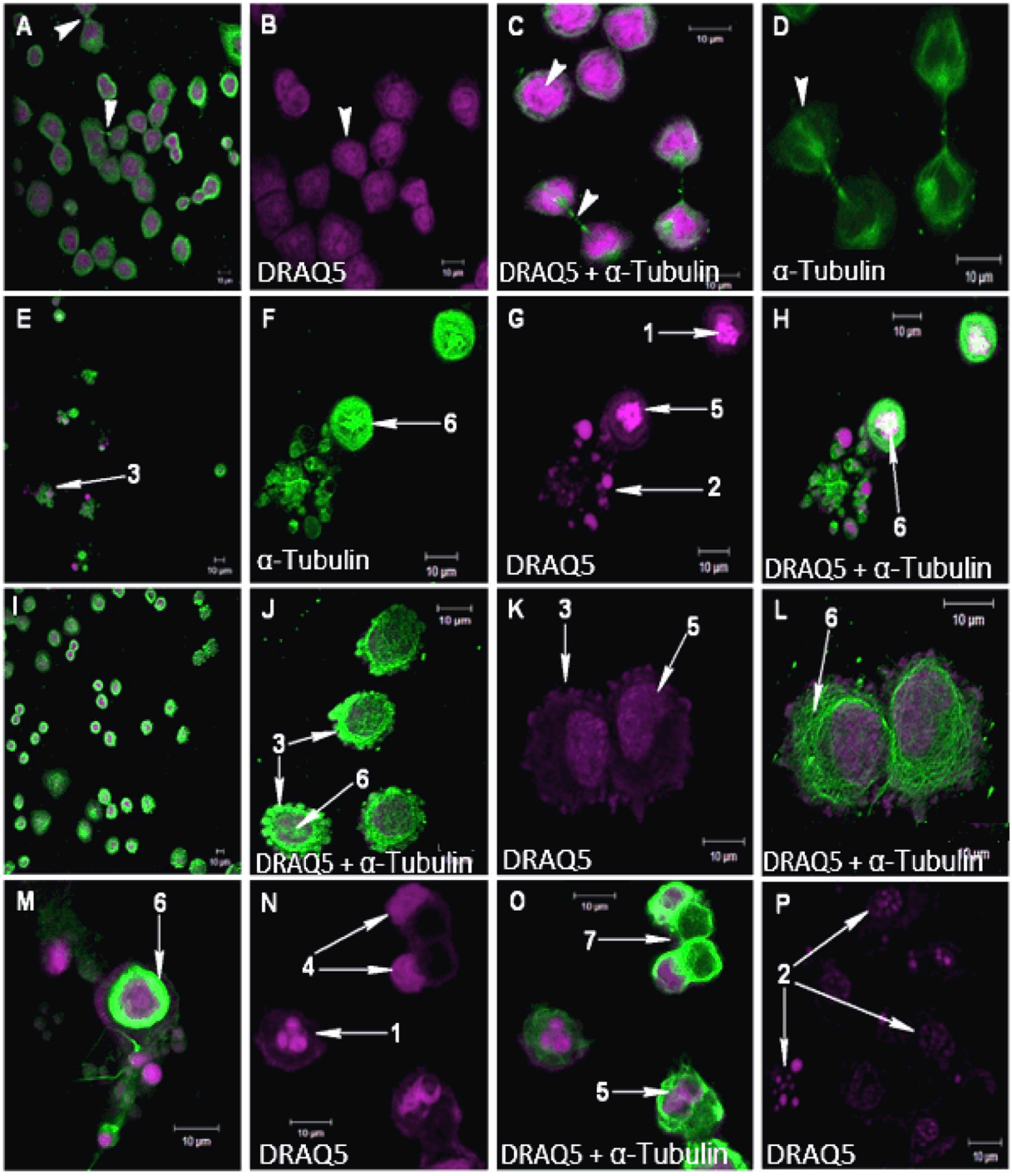

Fig. 11. Confocal microscopic illustrations of disruption in cytoskeletal architecture. Confocal microscopy illustrates the effects of CR and vincristine (24 h exposure) on MDA-MB-468 cell morphology. 1st row (**A–D**): untreated with vehicle only, arrowhead indicates typical morphology of nuclei, cell division and microtubule alignment; 2nd row (**E–H**): vincristine (10 nM); 3rd& 4th row (**I–P**): CR (1 × GI_{50} = 73.7 nM). CR caused multinucleation (1), nuclear fragmentation (2), membrane blebbing (3), the lunate morphology of chromatin and chromatin condensation (4), membrane disruption of nuclei (5), tubulin network disruption (6) and uneven cell division (7). CR and vincristine both showing similarity in induced morphological changes. The experiments were repeated 3 times. Cells were immunostained with an antibody specific for α-Tubulin (green) and counterstained with DRAQ5 (purple). (For interpretation of the references to colour in this figure legend, the reader is referred to the Web version of this article.)

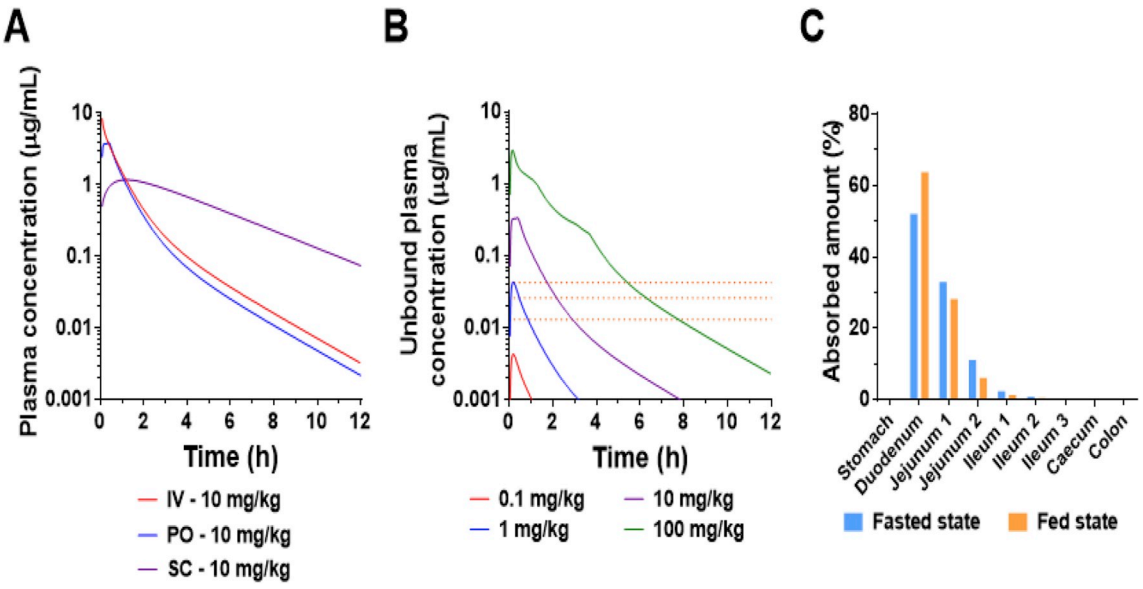

Fig. 12. *In silico* simulation of pharmacokinetics of CR in mice. (**A**) Predicted plasma concentration of cerberin following intravenous, oral and subcutaneous administration at 10 mg/kg. (**B**) Predicted unbound concentration of cerberin in plasma following oral administration at a range of doses. The orange dotted lines are the GI_{50} values of CR obtained in this study for MDA-MB-468, A549 and PANC-1 cell lines, respectively, from top to bottom. (**C**) Amount of cerberin predicted to be absorbed in each compartment of the gastrointestinal tract following oral administration of cerberin at 10 mg/kg in fasted or fed state. (For interpretation of the references to colour in this figure legend, the reader is referred to the Web version of this article.)

Table 3
Predicted pharmacokinetic parameters of CR following intravenous, oral and subcutaneous administration at 10 mg/kg in mice.

Parameters	Route of administration		
	Intravenous	Oral	Subcutaneous
F_a	–	99.9	–
F	–	61.2	96.6
C_{max} (µg/mL)	12.3	3.9	1.2
T_{max} (h)	–	0.4	1.2
AUC_{inf} (µg·h/mL)	6.3	3.9	6.1
CL_h (mL/h)	39.0		
CL_r (mL/h)	1.0		

F_a, fraction absorbed; F, bioavailability; C_{max}, maximum concentration in plasma; T_{max}, time of maximum concentration in plasma; AUC_{inf}, area under the concentration-time curve from time zero to infinity; CL_h, hepatic clearance; CL_r, renal clearance.

Appendix A. Supplementary data

Supplementary data to this article can be found online at https://doi.org/10.1016/j.canlet.2019.03.034.

Funding

This research did not receive any specific grant from funding agencies in the public, commercial, or not-for-profit sectors.

References

[1] F. Bray, J. Ferlay, I. Soerjomataram, R.L. Siegel, L.A. Torre, A. Jemal, Global cancer statistics 2018: GLOBOCAN estimates of incidence and mortality worldwide for 36 cancers in 185 countries, CA A Cancer J. Clin. 68 (2018) 394–424, https://doi.org/10.3322/caac.21492.

[2] C. Twelves, M. Jove, A. Gombos, A. Awada, Cytotoxic chemotherapy: still the mainstay of clinical practice for all subtypes metastatic breast cancer, Crit. Rev. Oncol. Hematol. 100 (2016) 74–87, https://doi.org/10.1016/j.critrevonc.2016.01.021.

[3] H. Rumpold, T. Winder, Development of chemotherapeutics in oncology: is there anything new? Memo - Mag. Eur. Med. Oncol. 10 (2017) 119–120, https://doi.org/10.1007/s12254-017-0350-4.

[4] D.J. Newman, G.M. Cragg, Natural products as sources of new drugs over the 30 years from 1981 to 2014, J. Nat. Prod. 79 (2016) 629–661, https://doi.org/10.1021/np200906s.

[5] F. Abe, H. Okabe, T. Yamauchi, Studies on Cerbera. II. Cerbinal and its derivatives, yellow pigments in the bark of Cerbera manghas L. Chem. Pharm. Bull. (Tokyo). 25 (1977) 3422–3424, https://doi.org/10.1248/cpb.25.3422.

[6] C. Wiart, Medicinal Plants of the Asia-Pacific, WORLD SCIENTIFIC, 2006, https://doi.org/10.1142/5834.

[7] Y. Gaillard, A. Krishnamoorthy, F. Bevalot, *Cerbera odollam*: a 'suicide tree' and cause of death in the state of Kerala, India, J. Ethnopharmacol. 95 (2004) 123–126, https://doi.org/10.1016/j.jep.2004.08.004.

[8] S. Laphookhieo, S. Cheenpracha, C. Karalai, S. Chantrapromma, Y. Rat-a-pa, C. Ponglimanont, K. Chantrapromma, Cytotoxic cardenolide glycoside from the seeds of *Cerbera odollam*, Phytochemistry 65 (2004) 507–510, https://doi.org/10.1016/j.phytochem.2003.10.019.

[9] S. Cheenpracha, C. Karalai, Y. Rat-A-Pa, C. Ponglimanont, K. Chantrapromma, New cytotoxic cardenolide glycoside from the seeds of *Cerbera manghas*, Chem. Pharm. Bull. (Tokyo) 52 (2004) 1023–1025 doi:JST.JSTAGE/cpb/52.1023 [pii].

[10] S. Wen, Y. Chen, Y. Lu, Y. Wang, L. Ding, M. Jiang, Cardenolides from the Apocynaceae family and their anticancer activity, Fitoterapia 112 (2016) 74–84, https://doi.org/10.1016/j.fitote.2016.04.023.

[11] L.C. Chang, J.J. Gills, K.P.L. Bhat, L. Luyengi, N.R. Farnsworth, J.M. Pezzuto, A.D. Kinghorn, Activity-guided isolation of constituents of *Cerbera manghas* with antiproliferative and antiestrogenic activities, Bioorg. Med. Chem. Lett 10 (2000) 2431–2434, https://doi.org/10.1016/S0960-894X(00)00477-7.

[12] J. Carlier, J.Ô. Guitton, F. Bévalot, L. Fanton, Y. Gaillard, The principal toxic glycosidic steroids in *Cerbera manghas* L. seeds: identification of cerberin, neriifolin, tanghinin and deacetyltanghinin by UHPLC-HRMS/MS, quantification by UHPLC-PDA-MS, J. Chromatogr. B Anal. Technol. Biomed. Life Sci. 962 (2014) 1–8, https://doi.org/10.1016/j.jchromb.2014.05.014.

[13] M. Ehle, C. Patel, R.P. Giugliano, Digoxin: clinical highlights, crit. pathways cardiol, J. Evidence-based Med. 10 (2011) 93–98, https://doi.org/10.1097/HPC.0b013e318221e7dd.

[14] L. Menger, E. Vacchelli, O. Kepp, A. Eggermont, E. Tartour, L. Zitvogel, G. Kroemer, L. Galluzzi, Trial watch: cardiac glycosides and cancer therapy, OncoImmunology 2 (2013) e23082, , https://doi.org/10.4161/onci.23082.

[15] V. Kaushik, N. Azad, J.S. Yakisich, A.K. V Iyer, Antitumor effects of naturally occurring cardiac glycosides convallatoxin and peruvoside on human ER + and triple-negative breast cancers, Cell Death Dis. 3 (2017) 17009, https://doi.org/10.1038/cddiscovery.2017.9.

[16] J.M. Calderón-Montaño, E. Burgos-Morón, M.L. Orta, D. Maldonado-Navas, I. García-Domínguez, M. López-Lázaro, Evaluating the cancer therapeutic potential of cardiac glycosides, BioMed Res. Int. 2014 (2014) 1–9, https://doi.org/10.1155/2014/794930.

[17] P. Babula, M. Masarik, V. Adam, I. Provaznik, R. Kizek, From Na^+/K^+-ATPase and cardiac glycosides to cytotoxicity and cancer treatment, Anti Cancer Agents Med. Chem. 13 (2013) 1069–1087, https://doi.org/10.2174/18715206113139990304.

[18] D.P. Huang, J.H.C. Ho, Y.F. Poon, E.C. Chew, D. Saw, M. Lui, C.L. Li, L.S. Mak, S.H. Lai, W.H. Lau, Establishment of a cell line (NPC/HK1) from a differentiated squamous carcinoma of the nasopharynx, Int. J. Cancer 26 (1980) 127–132, https://doi.org/10.1002/ijc.2910260202.
[19] M.E. Qazzaz, V.J. Raja, K.H. Lim, T.S. Kam, J.B. Lee, P. Gershkovich, T.D. Bradshaw, In vitro anticancer properties and biological evaluation of novel natural alkaloid jerantinine B, Cancer Lett. 370 (2016) 185–197, https://doi.org/10.1016/j.canlet.2015.10.013.
[20] T. Mosmann, Rapid colorimetric assay for cellular growth and survival: application to proliferation and cytotoxicity assays, J. Immunol. Methods 65 (1983) 55–63, https://doi.org/10.1016/0022-1759(83)90303-4.
[21] V.J. Raja, K.H. Lim, C.O. Leong, T.S. Kam, T.D. Bradshaw, Novel antitumour indole alkaloid, Jerantinine A, evokes potent G2/M cell cycle arrest targeting microtubules, Investig. New Drugs 32 (2014) 838–850, https://doi.org/10.1007/s10637-014-0126-1.
[22] N.A.P. Franken, H.M. Rodermond, J. Stap, J. Haveman, C. van Bree, Clonogenic assay of cells in vitro, Nat. Protoc. 1 (2006) 2315–2319, https://doi.org/10.1038/nprot.2006.339.
[23] M.K. Bin Break, M.S. Hossan, Y. Khoo, M.E. Qazzaz, M.Z.K. Al-Hayali, S.C. Chow, C. Wiart, T.D. Bradshaw, H. Collins, T.J. Khoo, Discovery of a highly active anticancer analogue of cardamonin that acts as an inducer of caspase-dependent apoptosis and modulator of the mTOR pathway, Fitoterapia 125 (2018) 161–173, https://doi.org/10.1016/j.fitote.2018.01.006.
[24] E.P. Rogakou, D.R. Pilch, A.H. Orr, V.S. Ivanova, W.M. Bonner, Double-stranded brekas induce histone H2AX phosphorylation on serine 139, J. Biol. Chem. 273 (1998) 5858–5868, https://doi.org/10.1074/jbc.273.10.5858.
[25] V.J. Raja, Biological Characterisation of a Novel and Naturally Isolated Indole Alkaloid, (2015) http://eprints.nottingham.ac.uk/29864/.
[26] E. Harlow, D. Lane, Bradford assay, Cold Spring Harb. Protoc. 2006 (2006), https://doi.org/10.1101/pdb.prot4644 pdb.prot4644-pdb.prot4644.
[27] T. Mahmood, P.C. Yang, Western blot: technique, theory, and trouble shooting, N. Am. J. Med. Sci. 4 (2012) 429–434, https://doi.org/10.4103/1947-2714.100998.
[28] H.M. Collins, M.K. Abdelghany, M. Messmer, B. Yue, S.E. Deeves, K.B. Kindle, K. Mantelingu, A. Aslam, G.S. Winkler, T.K. Kundu, D.M. Heery, Differential effects of garcinol and curcumin on histone and p53 modifications in tumour cells, BMC Canc. 13 (2013), https://doi.org/10.1186/1471-2407-13-37.
[29] Z. Xiao-po, P. Yue-hu, L. Ming-sheng, K. Sheng-li, Z. Jun-qing, Chemical constituents from the leaves of *Cerbera manghas*, Asian Pac. J. Trop. Med. 3 (2010) 109–111, https://doi.org/10.1016/S1995-7645(10)60046-6.
[30] F. Abe, T. Yamauchi, Studies on Cerbera. I. Cardiac glycosides in the seeds, bark, and leaves of *Cerbera manghas* L. Chem. Pharm. Bull. (Tokyo) 25 (1977) 2744–2748, https://doi.org/10.1248/cpb.25.2744.
[31] T. Yamuchi, Cerbera. III. Cardenolide monoglycosides from the leaves of Cerbera odollam and *Cerbera manghas*, Chem. Pharm. Bull. (Tokyo). 35 (1987) 2744–2749, https://doi.org/10.1248/cpb.35.2744.
[32] N.F.Z. Schneider, C. Cerella, J.-Y. Lee, A. Mazumder, K.R. Kim, A. de Carvalho, J. Munkert, R.M. Pádua, W. Kreis, K.-W. Kim, C. Christov, M. Dicato, H.-J. Kim, B.W. Han, F.C. Braga, C.M.O. Simões, M. Diederich, Cardiac glycoside glucoevatromonoside induces cancer Type-Specific cell death, Front. Pharmacol. 9 (2018) 1–17, https://doi.org/10.3389/fphar.2018.00070.
[33] S.L. Ham, S. Nasrollahi, K.N. Shah, A. Soltisz, S. Paruchuri, Y.H. Yun, G.D. Luker, A. Bishayee, H. Tavana, Phytochemicals potently inhibit migration of metastatic breast cancer cells, Integr, Biol. 7 (2015) 792–800, https://doi.org/10.1039/C5IB00121H.
[34] M.R. Sheen, J.D. Marotti, M.J. Allegrezza, M. Rutkowski, J.R. Conejo-Garcia, S. Fiering, Constitutively activated PI3K accelerates tumor initiation and modifies histopathology of breast cancer, Oncogenesis (2016), https://doi.org/10.1038/oncsis.2016.65.
[35] S.R. Kim, H.S. Seo, H.-S. Choi, S.-G. Cho, Y.K. Kim, E.H. Hong, Y.C. Shin, S.-G. Ko, *Trichosanthes kirilowii* ethanol Eetract and cucurbitacin D inhibit cell growth and induce apoptosis through inhibition of STAT3 activity in breast cancer cells, Evid. Based. Complement. Alternat. Med. 2013 (2013) 975350, https://doi.org/10.1155/2013/975350.
[36] W. Jiang, S. Kim, X. Zhang, R.A. Lionberger, B.M. Davit, D.P. Conner, L.X. Yu, The role of predictive biopharmaceutical modeling and simulation in drug development and regulatory evaluation, Int. J. Pharm. 418 (2011) 151–160, https://doi.org/10.1016/j.ijpharm.2011.07.024.
[37] M.D. Hämäläinen, A. Frostell-Karlsson, Predicting the intestinal absorption potential of hits and leads, Drug Discov. Today Technol. 1 (2004) 397–405, https://doi.org/10.1016/j.ddtec.2004.09.004.
[38] N.A. Hosea, H.M. Jones, Predicting pharmacokinetic profiles using in silico derived parameters, Mol. Pharm. 10 (2013) 1207–1215, https://doi.org/10.1021/mp300482w.
[39] L. Revue, P. Industries, T. Metabolic, T.E. Commission, T. European, D. a Smith, L. Di, E.H. Kerns, The effect of plasma protein binding on in vivo efficacy: misconceptions in drug discovery, Nat. Rev. Drug Discov. 9 (2010) 929–939, https://doi.org/10.1038/nrd3287.
[40] V. Pongrakhananon, Anticancer properties of cardiac glycosides, Cancer Treat. - Conv. Innov. Approaches (2013) 618, https://doi.org/10.5772/45937.
[41] A. Özdemir, B. İbişoğlu, Y.D. Şimay, B. Polat, M. Ark, Ouabain induces Rho-dependent rock activation and membrane blebbing in cultured endothelial cells, Mol. Biol. 49 (2015) 138–143, https://doi.org/10.1134/S0026893315010136.
[42] D.J. Radford, A.D. Gillies, J.A. Hinds, P. Duffy, Naturally occurring cardiac glycosides, Med. J. Aust. 144 (1986) 540–544, https://doi.org/10.1016/0378-8741(87)90017-1.
[43] I. Prassas, E.P. Diamandis, Novel therapeutic applications of cardiac glycosides, Nat. Rev. Drug Discov. 7 (2008) 926–935, https://doi.org/10.1038/nrd2682.
[44] D.G. Garcia, H.C. de Castro-Faria-Neto, C.I. da Silva, K.F.C. de Souza e Souza, C.F. Gonçalves-de-Albuquerque, A.R. Silva, L.M. da F. de Amorim, A.S. Freire, R.E. Santelli, L.P. Diniz, F.C.A. Gomes, M.V. de C. Faria, P. Burth, Na/K-ATPase as a target for anticancer drugs: studies with perillyl alcohol, Mol. Canc. 14 (2015) 105, https://doi.org/10.1186/s12943-015-0374-5.
[45] M. Diederich, F. Muller, C. Cerella, Cardiac glycosides: from molecular targets to immunogenic cell death, Biochem. Pharmacol. 125 (2017) 1–11, https://doi.org/10.1016/j.bcp.2016.08.017.
[46] M. Slingerland, C. Cerella, H.J. Guchelaar, M. Diederich, H. Gelderblom, Cardiac glycosides in cancer therapy: from preclinical investigations towards clinical trials, Investig. New Drugs 31 (2013) 1087–1094, https://doi.org/10.1007/s10637-013-9984-1.
[47] M. Mbele, R. Hull, Z. Dlamini, African medicinal plants and their derivatives: current efforts towards potential anti-cancer drugs, Exp. Mol. Pathol. 103 (2017) 121–134, https://doi.org/10.1016/j.yexmp.2017.08.002.
[48] D. Hanahan, R.A. Weinberg, Hallmarks of cancer: the next generation, Cell 144 (2011) 646–674, https://doi.org/10.1016/j.cell.2011.02.013.
[49] M.O. Hengartner, The biochemistry of apoptosis, Nature 407 (2000) 770–776, https://doi.org/10.1038/35037710.
[50] V.A. Fadok, D.L. Bratton, S.C. Frasch, M.L. Warner, P.M. Henson, The role of phosphatidylserine in recognition of apoptotic cells by phagocytes, Cell Death Differ. 5 (1998) 551–562, https://doi.org/10.1038/sj.cdd.4400404.
[51] L. Gong, Y. Tang, R. An, M. Lin, L. Chen, J. Du, RTN1-C mediates cerebral ischemia/reperfusion injury via ER stress and mitochondria-associated apoptosis pathways, Cell Death Dis. 8 (2017), https://doi.org/10.1038/cddis.2017.465 e3080.
[52] C. Lee, A. Fotovati, J. Triscott, J. Chen, C. Venugopal, A. Singhal, C. Dunham, J.M. Kerr, M. Verreault, S. Yip, H. Wakimoto, C. Jones, A. Jayanthan, A. Narendran, S.K. Singh, S.E. Dunn, Polo-Like Kinase 1 inhibition kills glioblastoma multiforme brain tumor cells in part through loss of SOX2 and delays tumor progression in mice, Stem Cell. 30 (2012) 1064–1075, https://doi.org/10.1002/stem.1081.
[53] C.M. Xie, X.Y. Liu, S. Yu, C.H.K. Cheng, Cardiac glycosides block cancer growth through HIF-1α-and NF-κb-mediated Plk1, Carcinogenesis 34 (2013) 1870–1880, https://doi.org/10.1093/carcin/bgt136.
[54] T. Mijatovic, N. De Neve, P. Gailly, V. Mathieu, B. Haibe-Kains, G. Bontempi, J. Lapeira, C. Decaestecker, V. Facchini, R. Kiss, Nucleolus and c-Myc: potential targets of cardenolide-mediated antitumor activity, Mol. Canc. Therapeut. 7 (2008) 1285–1296, https://doi.org/10.1158/1535-7163.MCT-07-2241.
[55] N. Sharma, R. Nanta, J. Sharma, S. Gunewardena, K.P. Singh, S. Shankar, R.K. Srivastava, PI3K/AKT/mTOR and sonic hedgehog pathways cooperate together to inhibit human pancreatic cancer stem cell characteristics and tumor growth, Oncotarget 6 (2015) 32039–32060, https://doi.org/10.18632/oncotarget.5055.
[56] P. Johnston, J. Grandis, STAT3 signaling: anticancer strategies and challenges, Mol. Inerventions. 11 (2011) 18–26, https://doi.org/10.1124/mi.11.1.4.
[57] Y. Qu, R. Zhao, H. Wang, K. Chang, X. Yang, X. Zhou, B. Dai, Y. Zhu, G. Shi, H. Zhang, D. Ye, Phosphorylated 4EBP1 is associated with tumor progression and poor prognosis in Xp11.2 translocation renal cell carcinoma, Sci. Rep. 6 (2016) 23594, https://doi.org/10.1038/srep23594.
[58] V.J. O'neill, C.J. Twelves, Oral cancer treatment: developments in chemotherapy and beyond, Br. J. Canc. 87 (2002) 933–937, https://doi.org/10.1038/sj.bjc.6600591.